


 Cite this: *RSC Adv.*, 2024, 14, 22894

# Molecular simulation of [P8883][Tf<sub>2</sub>N] ionic liquid decorated silica in 6FDA-ODA based mixed matrix membrane for enhanced CO<sub>2</sub>/CH<sub>4</sub> separation

 Mehtab Ali Darban,<sup>ab</sup> Serene Sow Mun Lock,<sup>id</sup> \*<sup>ab</sup> Suhaib Umer Ilyas,<sup>id</sup> <sup>c</sup>  
 Dun-Yen Kang,<sup>id</sup> <sup>d</sup> Mohd Hafiz Dzarfan Othman,<sup>e</sup> Chung Loong Yiin,<sup>id</sup> <sup>fg</sup>  
 Sharjeel Waqas<sup>b</sup> and Zunara Bashir<sup>ab</sup>

Mixed-matrix membranes (MMMs) have been reported to have considerable scope in gas separation applications because of their merged inherent strength of a durable polymer matrix and the exceptional performance capabilities of inorganic fillers. The selection of comparatively suitable polymers with fillers that can match each other and boost interfacial compatibility while ensuring uniform dispersion of filler within the polymer is still intensively demanding and is challenging at the experimental scale. Ionic liquids (ILs) are effective in promoting better dispersion and compatibility, leading to improved separation performance. A computational molecular simulation approach is employed in current work to design a hybrid membrane having Trioctapropyl phosphonium bis(trifluoromethylsulfonyl)imide [P8883][Tf<sub>2</sub>N] IL decorated silica as a filler and 4,4'-(hexafluoroisopropylidene)diphthalic anhydride-4,4'-oxydianiline (6FDA-ODA) polymer for carbon dioxide (CO<sub>2</sub>) separation from methane (CH<sub>4</sub>). Thermophysical and gas transport properties under pure and mixed gas condition (30, 50, and 70% CO<sub>2</sub>/CH<sub>4</sub>) within the MMMs with varying filler loadings (5, 10, and 15 wt% IL-silica) are examined *via* Grand Canonical Monte Carlo (GCMC) and Molecular Dynamics (MD) simulations. Membrane characteristics like glass transition temperature (*T*<sub>g</sub>), Fractional Free Volume (*v*<sub>f</sub>), X-Ray Diffraction (XRD), solubility, diffusivity, permeability, and selectivity for neat and IL-silica filled 6FDA-ODA are computed. The results show that the *T*<sub>g</sub> of the composite membrane with 5 wt% IL-silica is found to be considerably higher (with 305 °C) than that of the pure 6FDA-ODA polymer having 298 °C. A higher *T*<sub>g</sub> value highlights the effective dispersion and higher adhesion between the filler and polymer membrane. Additionally, CO<sub>2</sub> permeability for 5 wt% IL-silica/6FDA-ODA MMM is significantly improved, measuring 319.0 barrer while maintaining a CO<sub>2</sub>/CH<sub>4</sub> selectivity of 16.2. These values are 89% and 56% respectively, greater than the corresponding values of neat 6FDA-ODA membrane. Published data from the literature review is used to validate the findings and guarantee their reliability. The obtained results exhibited an error in the range of 0.7–9%. Hence, it is concluded from the study that molecular simulation can be used to design IL decorated silica incorporated within 6FDA-ODA matrix, which is able to boost the interfacial compatibility, with elevated CO<sub>2</sub>/CH<sub>4</sub> selectivity and CO<sub>2</sub> permeability.

Received 17th April 2024

Accepted 31st May 2024

DOI: 10.1039/d4ra02851a

[rsc.li/rsc-advances](https://rsc.li/rsc-advances)

## 1 Introduction

Raw natural gas, a fuel source of considerable global importance, contains a high level of CO<sub>2</sub>, requires its purification to prevent issues such as pipeline degradation, increased

compression costs, reduced heating efficiency, and increased greenhouse gas emissions.<sup>1,2</sup> Among the various separation technologies, membrane separation offers several advantages, including environmental friendliness, simple fabrication, trouble-free application, low capital cost, low energy

<sup>a</sup>Centre of Carbon Capture, Utilisation and Storage (CCCUS), Universiti Teknologi PETRONAS, Seri Iskandar 32610, Malaysia. E-mail: [sowmun.lock@utp.edu.my](mailto:sowmun.lock@utp.edu.my)

<sup>b</sup>Department of Chemical Engineering, Universiti Teknologi PETRONAS, Seri Iskandar 32610, Malaysia

<sup>c</sup>Chemical Engineering Department, University of Jeddah, Jeddah 23890, Kingdom of Saudi Arabia

<sup>d</sup>Department of Chemical Engineering, National Taiwan University, Taipei 10617, Taiwan

<sup>e</sup>Advanced Membrane Technology Research Centre (AMTEC), Faculty of Chemical and Energy Engineering, Universiti Teknologi Malaysia (UTM), 81310, Skudai, Johor Bahru, Malaysia

<sup>f</sup>Department of Chemical Engineering and Energy Sustainability, Faculty of Engineering, Universiti Malaysia Sarawak (UNIMAS), 94300, Kota Samarahan, Sarawak, Malaysia

<sup>g</sup>Institute of Sustainable and Renewable Energy (ISuRE), Universiti Malaysia Sarawak (UNIMAS), 94300, Kota Samarahan, Sarawak, Malaysia



consumption, well-space utility, and excellent thermal suitability.<sup>3</sup> However, polymeric membranes have some shortcomings to meet industrialization standards due to the well-known “trade-off” between permeability and selectivity.<sup>4</sup>

Mixed matrix membranes (MMMs) are designed to exceed Robeson's upper bounds to get around the tradeoff between permeability and selectivity. MMMs consist of a polymer matrix with distributed inorganic components, allowing them to possess the advantageous characteristics of both inorganic and polymer membranes.<sup>5</sup> In the MMM, the dispersed inorganic filler disrupts the effective packing of polymer for the creation of void channels to facilitate gas transport while also enhancing affinity for a specific molecule to improve separation performance.<sup>6</sup> This gives MMMs a significant performance boost over a basic polymeric membrane.<sup>7</sup> However, improper filler dispersion and low interfacial compatibility between the filler and polymer led to a tradeoff between permeability and selectivity, common issues faced by MMM, causing a bottleneck in its further enhancement. To tackle this concern and improve CO<sub>2</sub>/CH<sub>4</sub> separation, supporting ionic liquids onto the surface of fillers or polymers has been proposed.<sup>8,9</sup>

To date, several studies have been conducted to support ionic liquids (ILs) on polymers and fillers to improve their CO<sub>2</sub> separation performance. There are various methods to support ILs on the surface of polymer and filler,<sup>10</sup> which encompass impregnation,<sup>11</sup> physical stirring,<sup>12</sup> supercritical fluid deposition (SCFD),<sup>13</sup> blending,<sup>14</sup> and grafting.<sup>15</sup> A study was conducted on the synthesis of Ethyl Cellulose (EC) supported with 1-carboxymethyl-3-methylimidazolium tetrafluoroborate [HOOC-MIM][BF<sub>4</sub>]. The resulting EC exhibited a permeability of 199 barrer, which was significantly higher than that of the pure EC (46.8 barrer). Furthermore, the selectivity for CO<sub>2</sub>/CH<sub>4</sub> increased from 9.0 to 19.<sup>16</sup> A. S. Aquino *et al.*<sup>17</sup> studied methyl-3-(3-trimethoxysilylpropyl) imidazolium chloride [MTMSP-Im][Cl] supported on mesoporous material (MCM-41) and found that at 25 °C and 1 bar, the CO<sub>2</sub> adsorption capacity of IL supported on MCM-41 was 57% higher than that of the bare MCM-41 with merely 0.62 mmol CO<sub>2</sub> per g sorbent. Wang *et al.*<sup>18</sup> synthesized 1-*n*-butyl-3-methylimidazolium chloride [BMIM][Cl] decorated Santa Barbara Amorphous-15 (SBA-15) and observed that under similar conditions, the CO<sub>2</sub> adsorption of SBA-15-IL was 63% higher than that of the neat SBA-15. Using the same method, Vishwanath Hiremath *et al.*<sup>19</sup> studied four amino acid (AA) functionalized 1-methyl-3-ethyl-imidazolium [EMIM] based IL supported on ordered mesoporous silica (OMS-IL (AA)) and compared its CO<sub>2</sub> sorption capacity with bare silica (0.11 mmol g<sup>-1</sup>). They observed that the CO<sub>2</sub> sorption capacity of OMS-IL (AA) was 63% higher than that of the neat silica. Bahadori *et al.*<sup>20</sup> prepared 1-(2-aminoethyl)-3-methyl imidazolium bromide [NH<sub>2</sub>-EMIM][Br] grafted on MIL-101(Cr) and found that the CO<sub>2</sub> sorption capacity of the grafted sample was 7.84 times higher than the MOFs present at that time. Zhu *et al.*<sup>15</sup> synthesized triocetapropyl phosphonium bis(triflimide) [P8883][Tf<sub>2</sub>N] grafted silica and obtained the CO<sub>2</sub> capture performance increased from 0.07 mmol g<sup>-1</sup> to 0.99 mmol g<sup>-1</sup>.

Preparing MMMs using the incorporation of IL modified filler in the polymeric matrix is another widely used method.

Ilyas *et al.*<sup>21</sup> conducted a study where they developed a mixed matrix membrane consisting of zeolite 4A filler supported by an IL called 3-(trimethoxysilyl)propan-1-aminium acetate [APTMS][AC] and polysulfone (PSF) polymer. Their research revealed that incorporating a filler content of 34 wt% in the membrane led to an enhanced separation performance. Specifically, the modified filler demonstrated an increase in the selectivity of CO<sub>2</sub>/CH<sub>4</sub> by 37% and CO<sub>2</sub>/N<sub>2</sub> by 43% as compared to the original unmodified filler in the MMMs. Li *et al.*<sup>22</sup> synthesized 1-butyl-3-methylimidazolium bis(triflimide) [Bmim][Tf<sub>2</sub>N] embedded in ZIF-8/Pebax-1657 based MMM and observed membrane performance at various loadings of [Bmim][Nf<sub>2</sub>T]@ZIF-8. They reported the highest CO<sub>2</sub> permeability of 104.9 barrer at 15 wt% loading, which was 28% greater than that of the pure Pebax-1657 (72 barrer) and the selectivity was also increased from 18 to 34.5. To separate CO<sub>2</sub> from CH<sub>4</sub> and N<sub>2</sub>, Ahmad *et al.*<sup>23</sup> employed 1-ethyl-3-methylimidazolium bis(triflimide) [EMIM][Tf<sub>2</sub>N] supported on zeolite SAPO-34, which was subsequently integrated into PSF. Compared to the unmodified MMM, they observed a substantial improvement in the CO<sub>2</sub> separation ability of a composite containing SAPO-34 modified with the IL, with an approximately 486% rise in CO<sub>2</sub>/CH<sub>4</sub> and a 232% increase in CO<sub>2</sub>/N<sub>2</sub> selectivity. Nevertheless, the process of identifying an appropriate filler and polymer that complement one another, as well as an ionic liquid that can enhance the surface-to-surface compatibility and propagation of the filler within the polymer, will inevitably involve numerous attempts and mistakes. Additionally, membrane morphology and performance of the new generation hybrid materials are difficult to measure *in situ*, causing testing of membranes on an experimental scale to be potentially costly, labor-intensive, and time-consuming. For instance, Liu *et al.*<sup>24</sup> synthesized a MMM consisting of a fluorinated metal organic framework (NbOFFIVE-1-Ni) filler and 4,4'-(hexafluoroisopropylidene) diphthalic anhydride-2,4,6-trimethyl-1,3-diaminobenzene (6FDA-DAM) polymer. The composite membrane (NbOFFIVE-1-Ni/6FDA-DAM) exhibited diminished CO<sub>2</sub>/CH<sub>4</sub> selectivity compared to the base 6FDA-DAM membrane, likely due to incompatibility between the polymer and filler materials.

Computational chemistry has grown as an effective tool that provides fast, atomistic-level elucidation of material properties in the creation and analysis of different materials. It offers modeling and simulation environment that can be used to anticipate and understand the connections between molecular structure of a material and its properties while circumventing the difficulty, cost, or time associated with lab-scale manufacturing.<sup>25,26</sup> Several computational studies have been conducted on polymers and MMMs. Velioğlu *et al.*<sup>27</sup> conducted a comprehensive investigation on the molecular simulation of gas transport on three distinct polyimides, namely 4,4-hexafluoroisopropylidene-diphthalic anhydride-2,4,6-trimethyl-*m*-phenylene diamine (6FDA-DAM), 4,4-hexafluoroisopropylidene-diphthalic anhydride-4,4-oxydianiline (6FDA-ODA), and 4,4-hexafluoroisopropylidene-diphthalic anhydride-2,5-dimethyl-*p*-phenylenediamine (6FDA-DPX). Their investigation involved the computation of diffusion and sorption coefficients of CO<sub>2</sub>, CH<sub>4</sub>, N<sub>2</sub>, and O<sub>2</sub> gases

within these polymers, employing simulation conditions of temperature and pressure set at 35 °C and 10 bar for CO<sub>2</sub> and CH<sub>4</sub>, and 35 °C and 2 bar for N<sub>2</sub> and O<sub>2</sub>. They were able to closely replicate the experimental findings. Karim *et al.*<sup>28</sup> conducted a simulation study on silica/PSF based mixed matrix membrane under pure gases condition, which included O<sub>2</sub>, N<sub>2</sub>, CO<sub>2</sub>, and CH<sub>4</sub> and observed that for 20 wt% silica, the CO<sub>2</sub> permeability was 22.5 barrer, which was 470% higher compared to permeability of pristine PSF (3.95 barrer) and the simulated results were in close agreement with the experimental values. Khadija *et al.*<sup>29</sup> further conducted molecular simulation study on CO<sub>2</sub>/CH<sub>4</sub> separation in silica/PSF based MMM. They varied silica filler loadings (15, 20, 25, and 30 wt%) to observe its effect on the gas transport properties of MMM and found that the permeability and selectivity were consistently increasing with incorporation of silica in PSF membrane until 25 wt%, which further decreased for 30 wt%. The same group later functionalized silica with amine and embedded it in PSF membrane and resulted optimum permeability (60 barrer) and selectivity (10.9) at 20% loading, which was higher than the unfunctionalized silica/PSF MMM.<sup>30</sup> Ban *et al.*<sup>31</sup> conducted experimental and molecular dynamic study on [Bmim][Tf<sub>2</sub>N]@ZIF-8/PSf MMMs and observed a significant enhancement in CO<sub>2</sub>/CH<sub>4</sub> separation performance. They found that with incorporation of 6 vol% of ionic liquid decorated filler, the CO<sub>2</sub> permeability increased from 228 to 307 barrer at 303 K and 6 bar. The selectivity also increased from 23.1 ± 2.6 to 36.9 ± 1.7 and both the simulation and experimental results were consistent. Hence, it can be concluded that a suitable computational model accurately predicts the separation capability of existing membranes and can subsequently be employed for the next generation membranes that can be used in macroscopic process simulation.

In summary, based on review of the literature, the supported IL membranes (SILMs) have higher gas separation performance than pristine polymeric membranes and IL-MMMs have even higher levels than SILMs. Instead of countless, expensive laboratory experiments, molecular simulation offers a virtual replica of a system, unlocking its unexplored properties. This not only saves time and money but also reduces the handling of hazardous materials.

Therefore, the objective of this study is to establish a computational structure for MMM that exhibits enhanced dispersion, compatibility, and separation capabilities. To accomplish this, a MMM consisting of an IL-decorated filler and a polymer is formulated. Due to prominent characteristics of polyimides, *i.e.*, outstanding thermal, chemical, and mechanical properties, as well as better CO<sub>2</sub>/CH<sub>4</sub> separation capabilities,<sup>32</sup> 6FDA-ODA polyimide has been employed as polymer in this study, while silica as a filler due to its prominent characteristics that can help to enhance the properties of gas transport (*i.e.*, permeability and selectivity<sup>33</sup>). Meanwhile, trioctapropyl phosphonium-bis(triflimide) [P8883][Tf<sub>2</sub>N] has been selected as an ionic liquid to decorate the silica filler, in which [Tf<sub>2</sub>N]<sup>+</sup> is favorable for CO<sub>2</sub> adsorption.<sup>34</sup> Along with this, phosphonium based ionic liquids (PILs) are more thermally stable,<sup>35</sup> stable towards nucleophilic and basic conditions,<sup>36</sup> have lower

densities than water, low viscosity, high productivity, and low manufacturing cost than the rest of the ILs.<sup>37</sup> The concept based on pre-modification technique is used to construct the MMM *via* molecular simulation approach through which first IL is supported on silica surface and then embedded into polymer matrix. Design *via* grafting method is used to support ionic liquid on silica surface as reported earlier,<sup>10,15</sup> in which ionic liquids are chemically supported, that not only maintains the porous structure and surface of the substrate, but also offers good affinity with CO<sub>2</sub>. In the grafting method, the cations present are mainly responsible for chemically modified ILs based adsorbents.<sup>38</sup>

To understand how varying gas concentration affects transport properties in a mixed gas system, the interaction between gas molecules and IL-silica/6FDA-ODA based MMM should be explored. Even though it has been demonstrated that for single gas (CO<sub>2</sub>, CH<sub>4</sub>, N<sub>2</sub>, H<sub>2</sub>, and O<sub>2</sub>), IL-filler concentration boosts the membrane's solubility and diffusion coefficient relative to its pristine membrane,<sup>39</sup> investigation under the mixed gas environment at molecular level, which reflects actual natural gas sweetening process is still unresolved. Therefore, this study investigated the effect of immobilization of IL [P8883][Tf<sub>2</sub>N] on silica surface with varying weight percentages (*i.e.*, 5, 10, and 15) on the permeation characteristics of CH<sub>4</sub>/CO<sub>2</sub> under single and a gas mixture of CO<sub>2</sub> and CH<sub>4</sub> (*i.e.*, 70, 50, and 30 vol.%) at constant temperature (40 °C) and pressure (1 atm). Therefore, the distinctive characteristic of this investigation is to develop an innovative composite membrane and to elucidate the impact of diverse concentrations of CO<sub>2</sub>/CH<sub>4</sub> on the transportation properties in IL-silica/6FDA-ODA founded MMMs at varying IL-silica loadings using molecular simulation.

## 2 Methodology

In this work, atomistic simulations were performed utilizing Materials Studio (MS). Interactions were represented by empirical models so as to develop the essential motion equations.<sup>40</sup> The configuration of the system is followed to record position of each atom.<sup>41–43</sup> This process generates the temporal trajectory of the system, which can be utilized to analyze membrane framework and behavioral properties through the application of computational mechanics techniques.<sup>44,45</sup> Khadija *et al.*,<sup>29</sup> Karim *et al.*,<sup>39</sup> and Ahn *et al.*<sup>46</sup> compared experimental and simulation data to authenticate the methodology employed in their investigation of gas movement behavior.

### 2.1 Force field

The term “force field” refers to a computational model used in molecular simulation to estimate the forces between and within molecules specifically in molecular mechanics or Monte Carlo simulations. The force field uses the functional form and parameter sets to determine the potential energy of a system of atoms.<sup>47</sup> To replicate a system precisely, a force field is utilized to generate a collection of model configurations that are strictly consistent with a fully quantum mechanical description.<sup>48–51</sup> The potential energy ( $\nu$ ) in the Condensed-phase Optimized

Molecular Potentials for Atomistic Simulation Studies (COMPASS) is represented by eqn (1).<sup>52</sup>

All the terms in the equation, with the exception of the final two terms, can be classified as valence terms. These terms are

with radius 6.1 Å is in accordance with the approach as reported by Karim,<sup>39</sup> while its ionic liquid modification mechanism is the same as described in the simulation by Khadija *et al.*<sup>30</sup> and experimentally by Zhu *et al.*,<sup>15</sup> and is shown in Fig. 2.

$$\begin{aligned}
 v = & \sum_b \left[ k_2^b (b - b_0)^2 + k_3^b (b - b_0)^3 + k_4^b (b - b_0)^4 \right] \\
 & + \sum_\theta \left[ k_2^\theta (\theta - \theta_0)^2 + k_3^\theta (\theta - \theta_0)^3 + k_4^\theta (\theta - \theta_0)^4 \right] \\
 & + \sum_\varnothing \left[ k_1^\varnothing (1 - \cos \varnothing) + k_2^\varnothing (1 - \cos 2\varnothing) + k_3^\varnothing (1 - \cos 3\varnothing) \right] \\
 & + \sum_x k_2^x x^2 + \sum_{b,b'} k^{b,b'} (b - b_0) (b' - b'_0) \\
 & + \sum_{b,\theta} k^{b\theta} (b - b_0) (\theta - \theta_0) + \sum_{b,\varnothing} (b - b_0) \left[ k_1^{b\varnothing} \cos \varnothing + k_2^{b\varnothing} \cos \varnothing + k_3^{b\varnothing} \cos 3\varnothing \right] \\
 & + \sum_{\theta,\varnothing} (\theta - \theta_0) \left[ k_1^{\theta\varnothing} \cos \varnothing + k_2^{\theta\varnothing} \cos \varnothing + k_3^{\theta\varnothing} \cos 3\varnothing \right] + \sum_{\theta,\theta'} k^{\theta,\theta'} (\theta - \theta_0) (\theta' - \theta'_0) \\
 & + \sum_{\theta,\theta',\varnothing} k^{\theta\theta'\varnothing} (\theta - \theta_0) (\theta' - \theta'_0) \cos \varnothing + \frac{1}{4\pi\epsilon_0} \sum_{ij} \frac{q_i q_j}{r_{ij}} + \sum_{ij} \epsilon_{ij} \left[ 2 \left( \frac{r_{ij}^0}{r_{ij}} \right)^9 - 3 \left( \frac{r_{ij}^0}{r_{ij}} \right)^6 \right]
 \end{aligned} \tag{1}$$

dependent on the lengths of bonds ( $b$ ), the angles between bonds ( $\theta$ ), the angles of torsion ( $\theta'$ ), or the out-of-plane angles ( $x$ ) formed by pair of atoms  $i$  and  $j$  that are bonded together. The inclusion of these terms is crucial for accurately predicting vibrational frequencies and variations in the geometry of bonded molecules that are connected to conformational changes.<sup>53</sup> In contrast, the last two terms are nonbonded interaction terms. These terms rely on the distances ( $r_{ij}$ ) between pairs of atoms that are separated by three or more bonds or that belong to different molecules. The coulombic contributions, which are dependent on the partial charges ( $q$ ) on atoms, play a vital role in the interactions between polar groups.<sup>54</sup> For homoatomic pairs, LJ-9-6 parameters ( $\epsilon_0$ ,  $r^0$ ) are provided.

The present study employed the COMPASS II force field,<sup>29,30</sup> which has exhibited notable efficacy in simulating polymeric systems.<sup>55,56</sup> The COMPASS model has been comprehensively parameterized for various organic and inorganic compounds.<sup>57</sup>

## 2.2 Molecular simulation on IL-silica/6FDA-ODA MMM

The first step for performing molecular simulation on MMM, was the construction of the polymer repeat unit. The 6FDA-ODA repeat unit, depicted in Fig. 1, was constructed utilizing the visualizer and collection module of MS following the method described by Velioglu *et al.*<sup>27</sup>

The length of the polymer chain was set to 20 repeat units as reported by Chen *et al.*<sup>48</sup> Shorter chains are better for ensuring an efficient physical system since they increase the polymeric chain's mobility regardless of the size of the cell.<sup>58,59</sup> The methodology for the construction of spherical  $\alpha$ -quartz silica

The second step is construction of the hybrid membrane structure using the amorphous cell module of MS. Before embedding the polymer chain and ionic liquid modified silica, the structures were subjected to energy minimization and geometry optimization using COMPASS II along with smart minimizer approach that combines the conjugate gradient, steepest descent and, Newton methods to optimize the geometry and minimize the energy of the system.<sup>60,61</sup> An amorphous cell was generated with an initial density ( $\text{g cm}^{-3}$ ) of 0.987, which accounted for 70% of the recognized experimental density of 6FDA-ODA.<sup>62-65</sup> A 2000-steps energy minimization was then performed to optimize the geometry and reduce the energy of the first created atomic structure to remove any unwanted interactions, such as overlaps and close contacts. The incorporation of ionic liquid modified silica into 6FDA-ODA polymer is shown in Fig. 3 with the atomic representations as: red: oxygen, white: hydrogen, dark grey: carbon, blue: nitrogen, yellow: sulfur, vivid orange: silicon, pale cyan: fluorine, and pale magenta: phosphorus.

The system was subsequently annealed utilizing the temperature cycle protocol implemented in the Forcite module. The system was subjected to temperature variations between 300.15 K and 553.15 K, which is considerably greater than the  $T_g$  value of the polymer,<sup>62</sup> and then cooled back at steps of 293.15 K. The cell was then subjected to 100 picosecond (ps) *NPT* dynamics at each step. To achieve stable structures and to evaluate whether the membrane system has reached an equilibrated condition that resembles properties similar to the real configuration, a 500 ps *NPT* ensemble MD was performed. The *NPT* ensemble maintains a constant quantity of particles ( $N$ ),



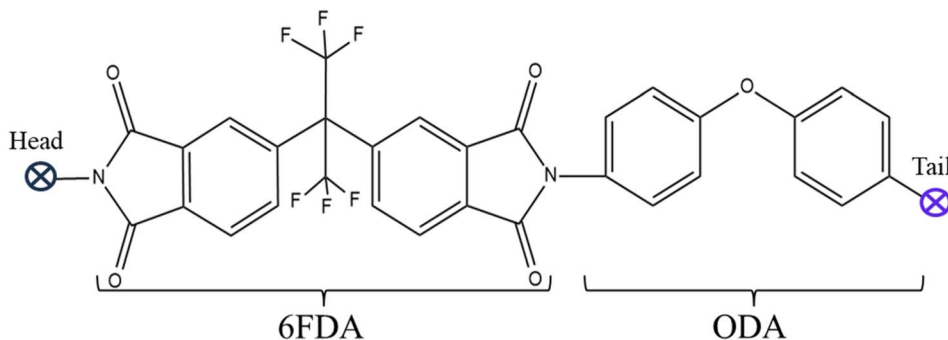


Fig. 1 The single chain structure of 6FDA-ODA repeat unit.

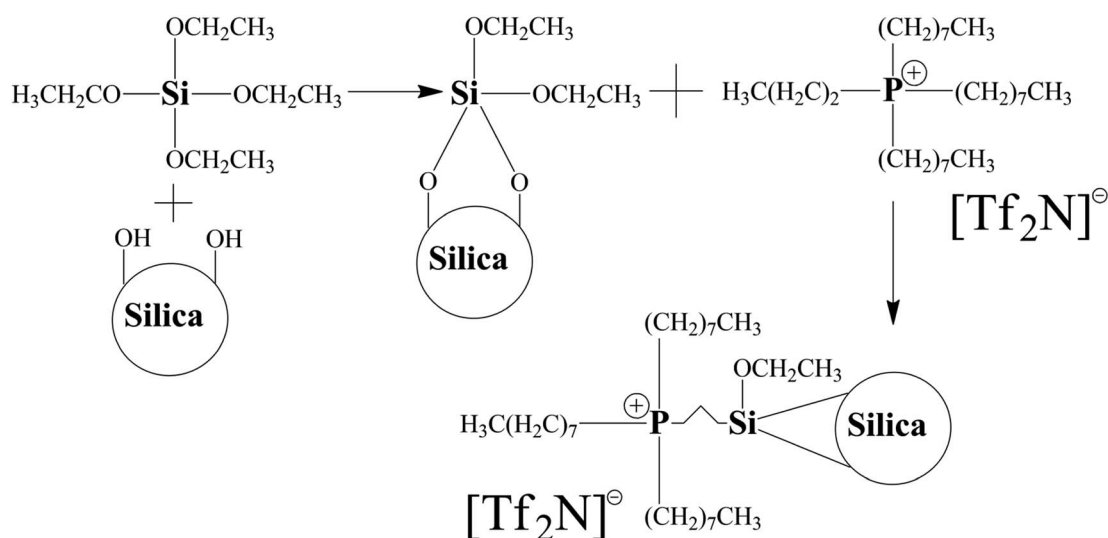


Fig. 2 Procedure to support IL on silica surface.

pressure ( $P$ , 1 atm), and temperature ( $T$ , 298.15 K). *NPT* thermodynamic package changes cell volume according to material to provide a realistic density of the material. Using the COMPASS II force field, non-bonded responses, including coulombic and van der Waals attractions, were computed. The Ewald model was employed to compute coulombic interactions with accuracy of  $0.0001 \text{ kcal mol}^{-1}$  while van der Waals interactions were considered using Lennard-Jones 9-6 function *via* atomic method. A Nose-Hoover thermostat and Bendersen barostat were used for controlling temperature and pressure, respectively, while maintaining the cutoff distance between 12.5 and 19 Å (less than half of the cell length) at a time step of 1 fs.<sup>27</sup>

In order to ascertain the stability of each structure, eqn (2) was utilized to derive the binding energy ( $E_b$ ).<sup>66</sup>

$$E_b = -E_1 = E_{\text{total}} - (E_{\text{polymer}} + E_{\text{IL-silica}}) \quad (2)$$

where  $E_b$  is the binding energy,  $E_{\text{total}}$  is the overall energy for the hybrid membrane structure,  $E_{\text{polymer}}$  shows energy of the polymer (6FDA-ODA), and  $E_{\text{IL-silica}}$  is energy of the IL-silica.

A fundamental characteristic of a more stable system is that it possesses a higher negative adhesive energy.<sup>67</sup> When the binding energy is negative, this indicates that the composite's total energy is less than the combined energy values of its

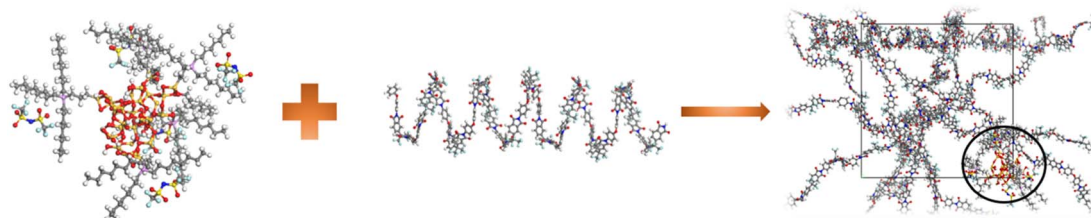


Fig. 3 Illustration of embedment of IL-silica into 6FDA-ODA polymer to form IL-silica/6FDA-ODA MMM amorphous cell.

constituent parts. Therefore, achieving a complicated system with increased stability is enabled. On the contrary, a system's intrinsic instability is indicated by positive binding energy. In sum, the stability of a membrane system is directly proportional to the decrease in its binding energy.<sup>68</sup>

### 2.3 Physical properties

The approach employed in this study to evaluate the physical parameters, such as the fractional free volume and X-ray diffraction pattern, and glass transition temperature ( $T_g$ ), is covered in the sections 2.3.1, 2.3.2, and 2.3.3, respectively.

**2.3.1 Fractional free volume ( $v_f$ ).** Free volume in a polymer is the volume of the total mass that is not occupied by the polymer chains themselves, which allows the movement of diffusing molecules.<sup>69</sup> It is commonly used to describe the spaces or pores between polymer strands. Connolly surface task, employing a probe radius of 0 nm, was utilized to determine the cell and van der Waals volumes.<sup>70</sup> Fractional free volume ( $v_f$ ) is ratio of estimated specific free volume and the polymer specific volume and can be calculated from group-contribution method as depicted in eqn (3):<sup>71</sup>

$$v_f = \frac{v - v_o}{v_o} \quad (3)$$

where  $v$  is polymer molar volume and  $v_o$  is molar occupied volume of the repeat unit of a polymer at 0 K and can be obtained from the van der Waals volume ( $v_{vdv}$ ) as provided in eqn (4):<sup>72</sup>

$$v_o = 1.3v_{vdv} \quad (4)$$

**2.3.2 X-ray diffraction (XRD) pattern.** The FORCITE Scattering Analysis module of MS is utilized to estimate the material's crystallography.<sup>30</sup> The XRD data was obtained using X-ray radiation with wavelength of 1.542 Å and  $2\theta$  ranging from 10 to 50°. The angle of diffraction is used to determine the difference among the atomic planes and can be calculated by using Bragg's law:

$$n\lambda = 2d \sin \theta \quad (5)$$

where  $n$  is number of beams,  $\theta$  is angle of diffracted beam,  $\lambda$  is wavelength of the incident beam, and  $d$  is the distance between the plane atoms, which is used to determine the crystallinity of the material by generating diffraction patterns.<sup>39</sup> The cutoff value, and the range of interest of  $2\theta$  are defined to generate an XRD graph. The cut off number specifies how often a data point is recorded throughout the span of the analysis.<sup>29</sup>

The diffracted intensity ( $I(Q)$ ) of beam for the XRD of the simulated membranes can be obtained in the periodic boundary state and is connected to the radial distribution function *via* a Fourier transform operation,<sup>73</sup> as shown in eqn (6):

$$I(Q) = \sum_i \sum_j \frac{f_i f_j (\sin Qr_{ij})}{Qr_{ik}} \quad (6)$$

where  $f_i$  and  $f_j$  are structure factor,  $r$  is distance between  $i$  and  $j$  atom and  $Q$  is scattering angle magnitude and can be calculated as:

$$Q = \frac{4\pi \sin \theta}{\lambda} \quad (7)$$

**2.3.3 Glass transition temperature.** The temperature at which an amorphous polymer material changes from a hard and somewhat brittle "glassy" state into a softer or rubbery state, which is similar to supercooled liquid, is known as the glass transition temperature ( $T_g$ ).<sup>39,74,75</sup>  $T_g$  of each polymer with an amorphous structure varies, and this property helps to distinguish the temperature range at which a polymer is thought to remain stable and maintain its mechanical properties.<sup>76</sup> After performing all the simulations, the final structure was cooled from 723 K to 473 K with steps of 293 K and the specific volume at different temperatures was recorded and plotted against temperature. The temperature at which an abrupt change in slope of a specific volume is observed is considered as glass transition temperature ( $T_g$ ) of the material. This similar procedure was applied to all structures to find their  $T_g$ .

### 2.4 Simulation of transport properties for gas

The elaboration on methodologies used to compute the gas transport properties, which include solubility, diffusivity, permeability, and selectivity, are covered in sections 2.4.1, 2.4.2, and 2.4.3.

**2.4.1 Solubility.** Grand Canonical Monte Carlo method (GCMC) was used to calculate solubility of a gas in a membrane. For this, amorphous cells were constructed embedding neat polymer chains or polymer with filler. For each molecule in the amorphous cell, the non-bonded energy was computed utilizing the COMPASS II force field. Using the same force field, both coulombic and van der Waals forces were employed to simulate the sorption process.<sup>77</sup> The probability of determining the concentration of the permeable gas was computed utilizing the energy difference ( $E$ ) of the before and after the configurations in the GCMC method.<sup>78</sup> A widely recognized Metropolis algorithm is employed to decide whether a gas molecule's movements should be accepted or rejected. The translational movement's acceptance probability for construction and destruction ( $P_{acc}$ ) was computed by displacing gas molecules randomly in all  $x$ ,  $y$ , and  $z$  directions, as per eqn (8):<sup>78</sup>

$$P_{acc(\text{old} \rightarrow \text{new})} = \min \left[ 1; \exp \left( \frac{-\Delta E}{KT} \pm \ln \frac{N_i KT}{f_i V} \right) \right] \quad (8)$$

where  $\Delta E$  is the sum of non-bonded potential terms,  $V$  is the volume of membrane cell,  $k$  is the Boltzmann's constant,  $f_i$  is the fugacity, and  $N_i$  is number of  $i$  components in the membrane.

The solubility for an equilibrated gas-polymer system is ratio of the concentration ( $C$ , measured in  $\text{cm}^3$  (STP) per  $\text{cm}^3$  polymer) to the pressure ( $P_i$ ) (or partial pressure for mixed gas system) of the gas  $i$ . Hence the solubility ( $S_i$ ) of gas in a membrane can be calculated as follows:<sup>79</sup>

$$S_i = \lim_{P \rightarrow 0} \left( \frac{C_i}{P_i} \right) \quad (9)$$

**2.4.2 Diffusivity.** The diffusivity, which determines with what rate the gas molecules can move within the polymer is another important parameter of the gas transport properties. In order to determine the diffusivity of individual gases through the final membrane constructions of pure 6FDA-ODA and IL-silica/6FDA-ODA nanocomposites, ten molecules of CO<sub>2</sub> and CH<sub>4</sub> were introduced. Geometry optimization and energy minimization stages were conducted prior to the embedding process. In order to attain equilibrated density, the most effective amorphous cell of every membrane, in conjunction with the penetrant gases, underwent relaxation process for 500 picoseconds *NPT* ensemble MD at constant temperature of 308.15 K and pressure 1 atm. Following this, we conducted an *NPT* ensemble MD simulation for a duration of 5000 ps using simulated membrane structures of a satisfactory density. As a result, the precise trajectory of the gas molecules within each cell could be detected. The Forcite mean square displacement (MSD) analysis module was utilized to record the trajectories at 5000 ps. The slope of the plot (MSD vs. time) was used to determine the diffusivity coefficients of the selected gas molecules. The diffusion coefficient at normal regime was calculated when the slope of the plot logarithmic MSD vs. time approached to unity and were calculated using the Einstein relation,<sup>39</sup> as shown in eqn (10):

$$D_i = \frac{1}{6N} \sum_{i=1}^N \langle |r_i(t) - r_i(o)|^2 \rangle \quad (10)$$

where  $D_i$  is diffusion coefficient of atom  $i$ ,  $N$  is the quantity of diffusing components, and  $|r_i(t) - r_i(o)|^2$  is average mean square displacement of atom  $i$  and  $r_i(t)$  and  $r_i(o)$  are position vectors, representing final and initial positions of atom  $i$ . The anomalous diffusion for different regimes is distinguished by using power-law.<sup>80,81</sup>

$$\Delta t \propto D_i t^N \quad (11)$$

Different diffusion regimes are distinguished based on the value of the exponent  $n$ :  $n = 1$ , a normal diffusion region, and anomalous regime for  $n \neq 1$ .

**2.4.3 Permeability & selectivity.** Transport of gases in the polymeric membranes is based on 'solution-diffusion' concept and the model were formulated in the 19th century by Graham and later by Mitchell.<sup>82</sup> The permeability is the product of solubility ( $S$ ) and diffusivity ( $D$ ), for  $i$  component can be calculated using eqn (12):<sup>83,84</sup>

$$P_i = S_i \times D_i \quad (12)$$

The selectivity of gas separation membranes is another significant property which can be defined as the ability of

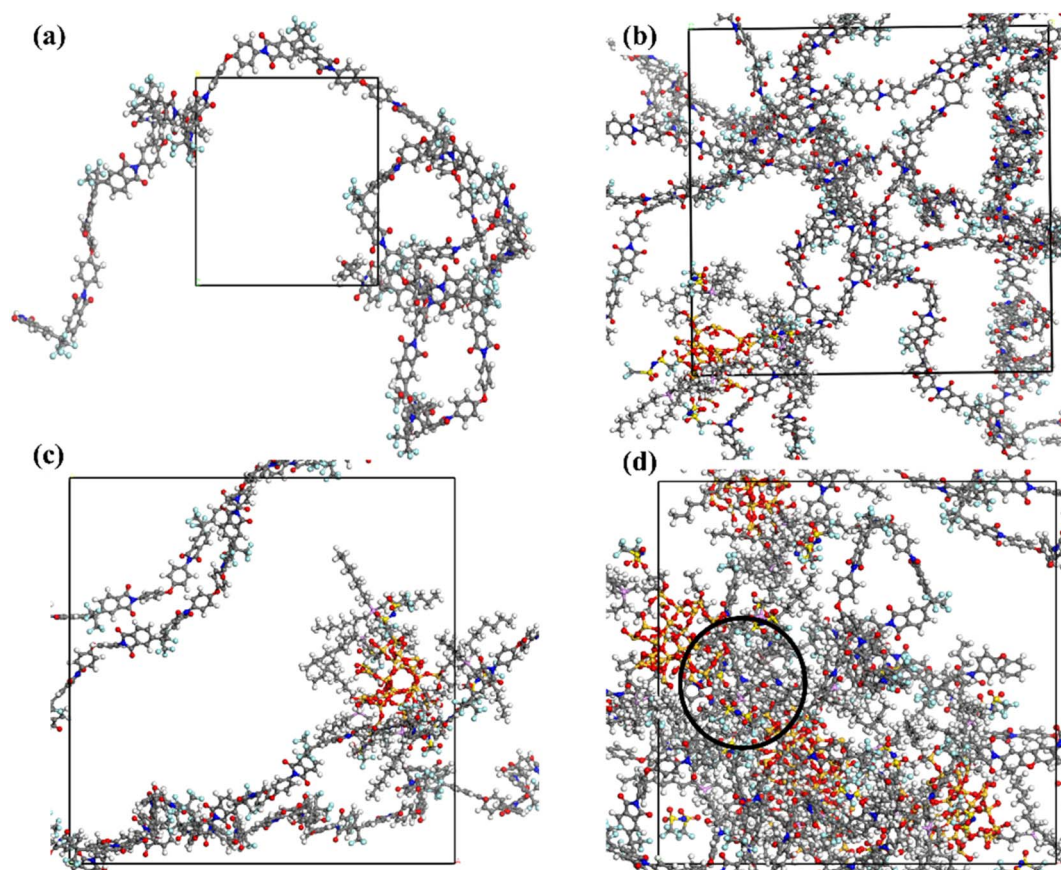


Fig. 4 Equilibrated amorphous cell for (a) neat 6FDA-ODA, (b) 5 wt% IL-silica/6FDA-ODA MMM, (c) 10 wt% IL-silica/6FDA-ODA MMM, (d) 15 wt% IL-silica/6FDA-ODA MMM.

a membrane to separate a gas from a gas mixture. According to this definition, the ideal selectivity is the ratio of the permeabilities of the gases<sup>85,86</sup> and can be calculated as follows:

$$\alpha_{ij} = P_i/P_j \quad (13)$$

where  $P_i$  and  $P_j$  are the permeabilities of two gases ( $i$  and  $j$ ) evaluated under similar conditions.

## 3 Results and discussions

### 3.1 Physical characteristics

**3.1.1 Equilibrated amorphous cells.** The amorphous cells for neat and incorporated ionic liquid modified silica in 6FDA-ODA co-polymer are illustrated in Fig. 4.

In order to authenticate the amorphous cells, the equilibrium density and potential and non-bonded energies status of the true membrane structures were applied. From Fig. 5(a) and (b), it was observed that after performing 500 ps *NPT* molecular dynamics, the system has acquired equilibrium. It was evident that the time-dependent curves of density and energy were approximately stable with fluctuations of <10% typically after 400 ps, suggesting that equilibrated structures had been achieved. The energy was minimized too during the molecular dynamic simulation process, suggesting evolution towards stable and equilibrated structures. The same judging methodology had been employed in previous published literature when evaluating the equilibrium time for their respective molecular dynamics simulation.<sup>87,88</sup> Additionally, the equilibrated density for neat 6FDA-ODA was  $1.39 \text{ g cm}^{-3}$ , which was in close agreement with experimental density ( $1.40 \text{ g cm}^{-3}$ ), yielding error of only 0.7%.<sup>89</sup> For 5 wt% of filler in simulated cell, the density decreased because of increased free volume. Conversely, the densities rose as the weight percentages of modified filler in simulated structures increased. The aforementioned effect was noted due to the filler's (silica) greater density ( $2.2 \text{ g cm}^{-3}$ ) in comparison to the 6FDA-ODA polymer. The minimal fluctuations in negative values of potential and non-bonded energy for an equilibrated system confirmed that the system is thermally

stable and has attained equilibrium as shown in Fig. 5(b). The potential and non-bonded energies of a membrane with 5 wt% IL-silica are lower than that of the pristine polymeric membrane which shows that the prior is more stable.

To further affirm stability of the system, the binding energy of the MMM with different wt% of IL-silica is calculated using eqn (2). As shown in Table 1, the binding energies of neat 6FDA-ODA and IL-silica were  $-459.26$  and  $-963.48 \text{ kcal mol}^{-1}$ , respectively. When 5 wt% IL-silica is added to 6FDA-ODA polymer, its binding energy was reduced to  $-9466.26 \text{ kcal mol}^{-1}$ . It was noted that a relatively more stable membrane system was achieved as MMM with 5 wt% IL-silica possessed 95% lower binding energy than the neat polymeric membrane. The octyl sidechain of the trioctapropyl phosphonium cation, which is chemically supported on the silica surface, is most likely oriented in a direction that is away from the silica surface. This nonpolar segment of the ionic liquid interacts with the nonpolar 6FDA-ODA polymer. Consequently, enhanced attraction between polymer and filler was achieved and hence stabilized the membrane system. For higher wt% of IL-silica the flexibility of the polymer increases consequently reduces the structure stability.

**3.1.2 Glass transition temperature ( $T_g$ ).** After having the optimized structure, it was cooled from  $450 \text{ }^\circ\text{C}$  to  $100 \text{ }^\circ\text{C}$  with steps of  $20 \text{ }^\circ\text{C}$  and the specific volume at different temperatures was recorded. For 6FDA-ODA membrane and 5 wt% IL-silica/6FDA-ODA MMM, Fig. 6 illustrates the variations in specific volume with respect to temperature.

After a linear increase in specific volume, an abrupt change was observed between  $250 \text{ }^\circ\text{C}$  and  $300 \text{ }^\circ\text{C}$ . The temperature at which an abrupt change in specific volume was observed is considered as the glass transition temperature ( $T_g$ ) of 6FDA-ODA and its IL-silica MMM. The obtained  $T_g$  results for neat 6FDA-ODA from simulation ( $298 \text{ }^\circ\text{C}$ ) were in close consistency with the experimental values ( $303 \text{ }^\circ\text{C}$ ) with 1.7% error. The simulated values of  $T_g$  for neat 6FDA-ODA and IL-silica/6FDA-ODA based MMM, calculated in similar way, are shown in Table 2.

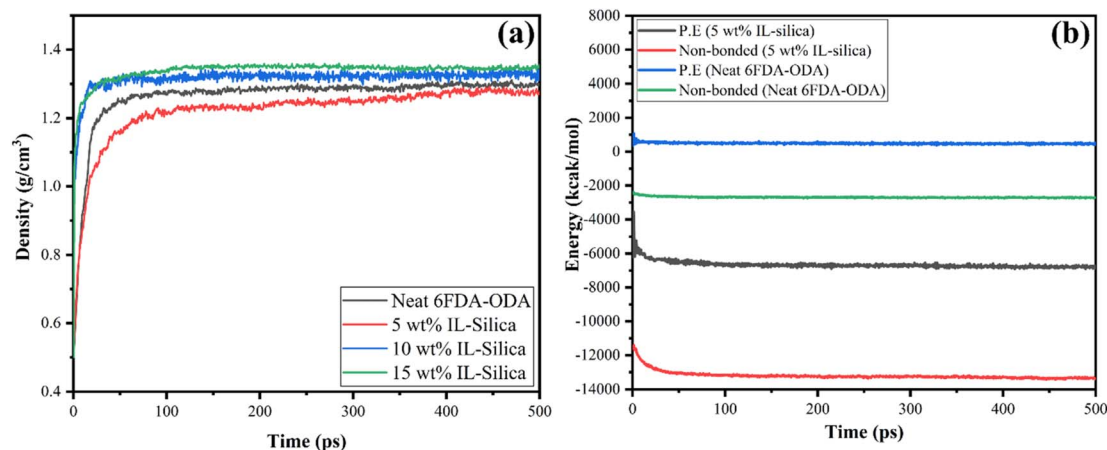
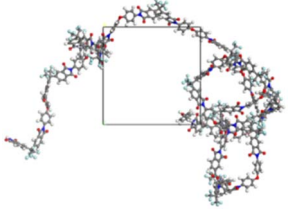
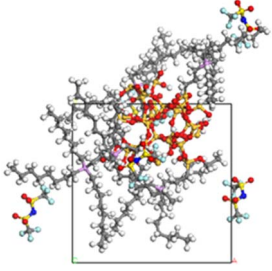
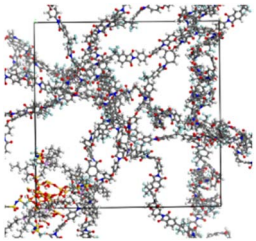
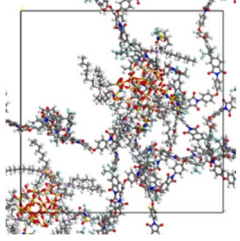
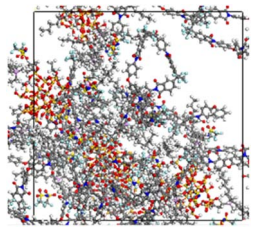


Fig. 5 Molecular dynamic simulation of (a) equilibrated density for all the structures; (b) potential and non-bonded energies for pristine polymeric membrane and 5 wt% IL-silica MMM.



Table 1 Binding energy of membrane systems consisting of different filler loadings

| Membrane         | Model system  | Total energy (kcal mol <sup>-1</sup> ) | Binding energy (kcal mol <sup>-1</sup> ) |
|------------------|---|--|--|
| Neat 6FDA-ODA    |    | -459.26                                | —  |
| IL-silica        |    | -963.48                                | —  |
| 5 wt% IL-silica  |    | -10889.83                              | -9466.26                                 |
| 10 wt% IL-silica |  | -2792.48                               | -1369.74                                 |
| 15 wt% IL-silica |  | -2100.47                               | -677.73                                  |

The  $T_g$  for neat 6FDA-ODA and 5 wt% IL-silica are 298 °C and 305 °C, respectively. An increase in the glass transition temperature ( $T_g$ ) for 5 wt% IL-silica supports the stability of the composite due to flat ring structure and polar CF<sub>3</sub> groups along the surface of 6FDA-ODA that allows IL-silica to be in close contact with it, which results in relatively stronger van der Waals interactions between polymer and filler. The recent studies on polymer–filler interactions called the surface polarity of filler and polymer as a key driving force to change interfacial interactions.<sup>91</sup> The glass transition temperature ( $T_g$ ) of the IL-silica/6FDA-ODA based MMM increased slightly in comparison to the pristine polymeric membrane. This

can also be related to the introduction of the filler, which leads to an increment in rigidity. However, the  $T_g$  further decreases with an increase in IL-filler content (10 and 15 wt%). This is because the IL not only enhanced the flexibility of the polymer matrices but also reduced the contact area between the two materials as can be seen in Fig. 4(d) (black circle).<sup>92</sup> Consequently, the  $T_g$  for higher contents of IL-silica decreased.<sup>81</sup> However, when compared to the pristine polymeric membrane, the 10 and 15 wt% IL-silica/6FDA-ODA based MMM exhibits a relatively higher  $T_g$  value. This behavior is supported by the decrease in binding energy as the weight fraction of IL-silica rose.

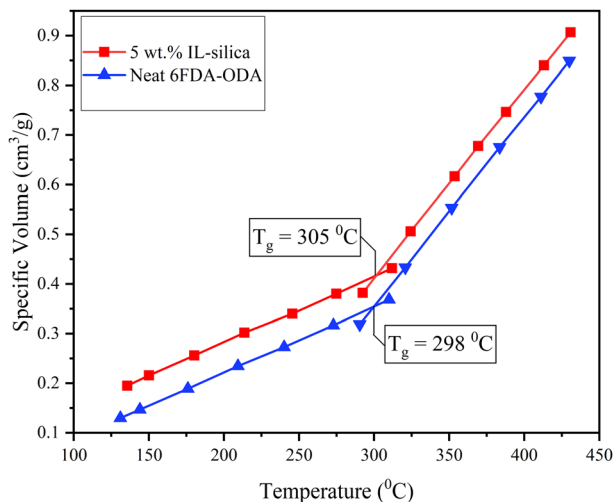


Fig. 6  $T_g$  of neat 6FDA-ODA and 5 wt% IL-silica/6FDA-ODA MMM.

**3.1.3 Fractional free volume ( $v_f$ ) in IL-silica/6FDA-ODA MMMs.** The transport mechanism of the permeable gas molecules in polymer membranes can be better understood with an understanding of the fractional free volume.<sup>93</sup>  $v_f$  for equilibrated IL-silica/6FDA-ODA MMM was averaged throughout the final five frames. The  $v_f$  values increased up to 40% (0.34 to 0.40) with incorporation of 5 wt% of IL-silica and then decreased in the following order: 10 wt%, 15 wt%, the similar effects on occupied and free volume are evident in the literature,<sup>31,89</sup> and is depicted in Fig. 7. The effective polymer packing creates gaps at the interface, which raises the free volume of the membrane structure that leads to improved gas transport.<sup>94,95</sup> The maximum free volume was recorded for incorporation of 5 wt% of IL-silica. For higher wt% (10 and 15) of IL-silica filler loadings, a notable reduction in free volume is observed because of the cavity occupation by ionic liquid. However, with not a considerable variation in the free volume values of IL-silica/6FDA-ODA MMMs are shown in Table 2.

For higher wt% of IL-silica (*i.e.*, 10 and 15 wt%), it is postulated that there exists a boundary free from defects between the dispersed particles and the polymer interface.<sup>96</sup> The robust adhesion between the polymer and filler leads to a decrease in the available volume within the polymer,<sup>97</sup> a phenomenon commonly referred to as polymer rigidification. In the majority of instances, this rigidification enhances the selectivity of the system while concurrently diminishing its permeability.<sup>98</sup>

**3.1.4 X-ray diffraction analysis.** The Forcite scattering module of the simulation software was used to find the XRD patterns of the neat 6FDA-ODA polymer and IL-silica filled 6FDA-ODA structures. Fig. 8 presents the XRD patterns of all simulated structures. 6FDA-ODA is an amorphous polymer since its structure lacks a regular arrangement. Several investigations indicate that the polymer chains of 6FDA-ODA are not tightly packed. This leads to the chains being challenging to organize in a consistent manner, resulting in the lack of a clearly defined, extensive arrangement in the structure.<sup>62,99–102</sup>

As the  $2\theta$  was varied from  $10^\circ$  to  $50^\circ$ , a sharp peak was generated for each membrane, indicating the crystalline region of the membrane. The main peak for neat 6FDA-ODA is at  $2\theta \approx 15.9^\circ$  which is well consistent with the published literature ( $15.5^\circ$ ) having a 2.6% error.<sup>102</sup> The diffraction peak for IL-silica filled structure coincided with the neat structure with a negligible shift in main peak. It was evident that the ionic liquid has the capability to disrupt the ordered arrangement of molecules in 6FDA-ODA, resulting in a lower degree of crystallinity in the membrane matrix by demonstrating decreased intensity of the XRD peak.<sup>103</sup> The peak got broader with increment in the IL-silica content and became flattened for 15 wt% IL-silica. A similar trend was observed in the previous studies.<sup>104–106</sup> Introducing the filler with IL decorated on its surface into the membrane matrix may potentially increase the free volume with efficient disruption in the polymer chain. However, the ionic liquid to be located between the polymer chains causes lubrication effect between the filler and the polymer, which can effectively avoid the aggregation of filler. Under such condition, the increment in  $d$ -spacing is not apparent when the filler amount is not sufficient. However, at higher amount of IL-modified silica, the  $2$ -theta is further shifted to the left and resulted bigger  $d$ -spacing values due to creation of more free volume.<sup>107</sup> The  $d$ -spacing values for the structures are calculated by using eqn (4) and are presented in Table 1.

## 3.2 Gas transport study

The majority of pressure-driven polymer membranes employ a solution–diffusion mechanism for gas transport, which are consisted of three stages: sorption, diffusion, and desorption. The gas molecules firstly adsorb on the polymer's upstream surface. Next, they diffuse through the membrane's pores, and lastly, they desorb on the membrane's downstream side.<sup>108–110</sup>

**3.2.1 Gas solubility  $\text{CO}_2/\text{CH}_4$ .** This section elucidates the sorption characteristics of IL-silica/polyimide-based

Table 2 Physical properties of 6FDA-ODA based membrane with varying weight percentages of IL-silica<sup>a</sup>

| Membrane | $T_g$ (°C) | Density ( $\text{g cm}^{-3}$ ) | Fractional free volume | $d$ -Spacing |
|----------|------------|--------------------------------|------------------------|--------------|
| 0        | 298 (303)  | 1.39 (1.40)                    | 0.34 (0.32)            | 5.57 (5.6)   |
| 5        | 305        | 1.21                           | 0.41                   | 5.87         |
| 10       | 301        | 1.41                           | 0.315                  | 6.11         |
| 15       | 300        | 1.43                           | 0.30                   | 6.25         |

<sup>a</sup> Experimental values are shown in brackets.<sup>89,90</sup>

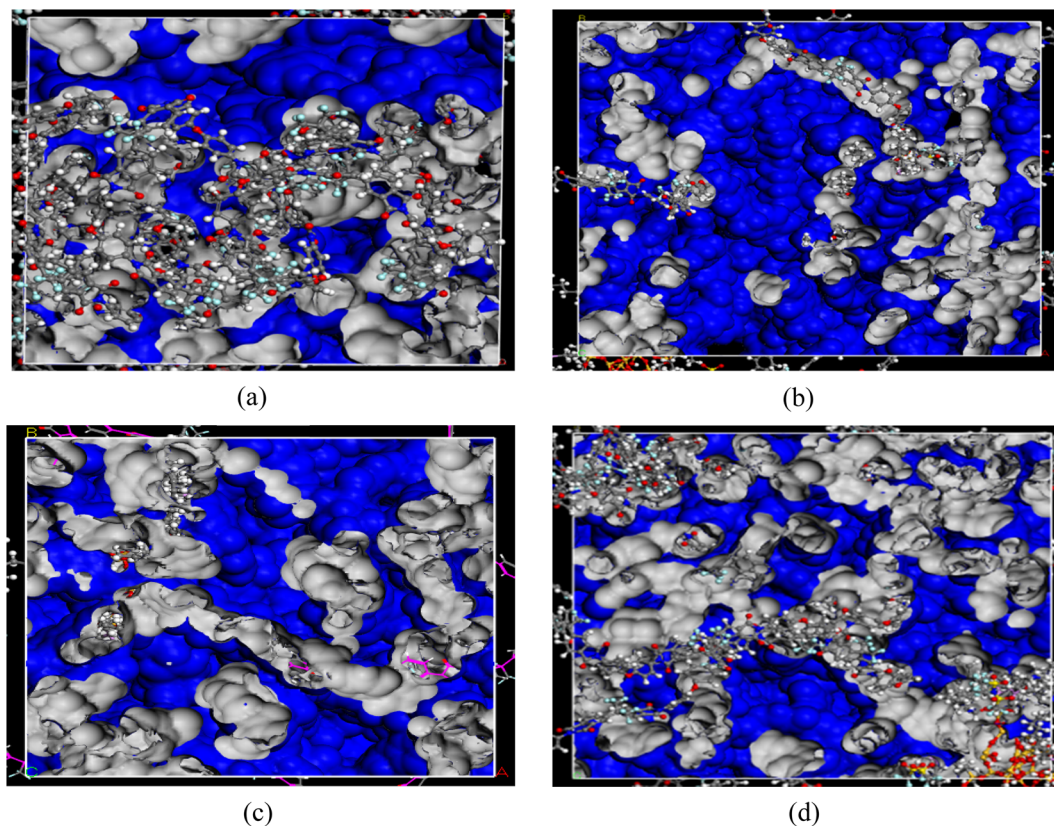


Fig. 7 Fractional free volume (a) for neat 6FDA-ODA (b) 5 wt% IL-silica (c) 10 wt% IL-silica (d) 15 wt% IL-silica.

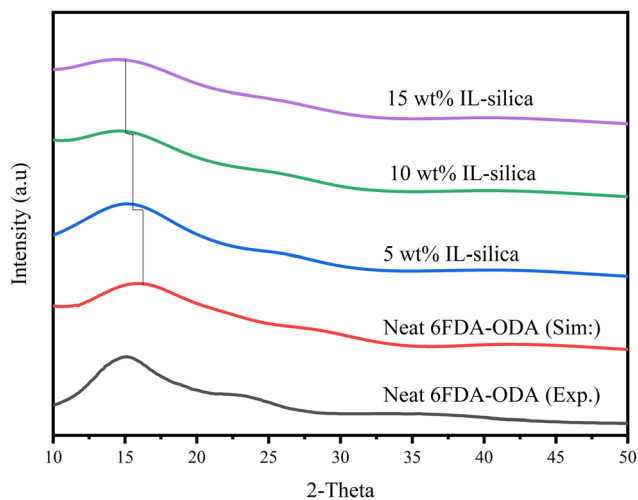


Fig. 8 X-ray scattering patterns for 6FDA-ODA polymer with different weight percentages of IL-silica (experimental XRD data for neat 6FDA-ODA is extracted from the graph<sup>89</sup>).

membranes with respect to gas molecules. The sorption module of the MS with utilizing the adsorption isotherm task has been performed to ascertain the solubility of gases within the membrane. The solubility results obtained for CO<sub>2</sub> in 6FDA-ODA (0.311 mmol g<sup>-1</sup>) and silica supported [P883][Tf<sub>2</sub>N] (0.74 mmol g<sup>-1</sup>) are consistent with the experimental data (0.33 mmol g<sup>-1</sup> at 35 °C and 1 bar (ref. 102) and 0.8 mmol g<sup>-1</sup> at 40 °C

and 1 atm,<sup>15</sup> with 5.7% and 7.5% error, respectively). Fig. 9 plots the predicted solubility and sorption energy distribution values for IL-silica/6FDA-ODA MMM structures for CO<sub>2</sub> and CH<sub>4</sub> in mixed and pure gas conditions at 40 °C and 1 atm and shows that CO<sub>2</sub> is more soluble than CH<sub>4</sub>, with solubility increasing in proportion to gas concentration within the membrane structure.

Fig. 9(a) demonstrates that CO<sub>2</sub> is more soluble than CH<sub>4</sub>. For all weight percentages of filler, the solubility results for pure gases were higher than the mixed gas conditions. This is because the pure gases have no competition for adsorption sites and uniform and well-defined interactions with the membranes over the mixed gases flowing through the membrane, shown in Fig. 9(e). Fig. 9(b) shows the largest density of CO<sub>2</sub> adsorbed onto interface between the silica surface and polymer chain. Fig. 9(d) shows two different absorption sites for CO<sub>2</sub> and CH<sub>4</sub> and is confirmed from different energy peaks for CO<sub>2</sub> (−6.8 kcal mol<sup>-1</sup>) and CH<sub>4</sub> (−4.8 kcal mol<sup>-1</sup>) shown in Fig. 9(c). The sorption capacity can go up if the energy distribution shows higher and wider peaks. This shows how the CO<sub>2</sub> and CH<sub>4</sub> sorbates interact with the membrane material.

The membrane with 5% weight percentage of filler showed the highest solubility for pure gas and mixed gas feed under 70% CO<sub>2</sub>. This pattern is in line with earlier research on the mixed gas trend of CO<sub>2</sub>/CH<sub>4</sub> because as the percentage of CO<sub>2</sub> in the membrane rises, it suppresses the route of CH<sub>4</sub> gas molecules.<sup>111</sup> Incorporation of ionic liquid modified silica into 6FDA-



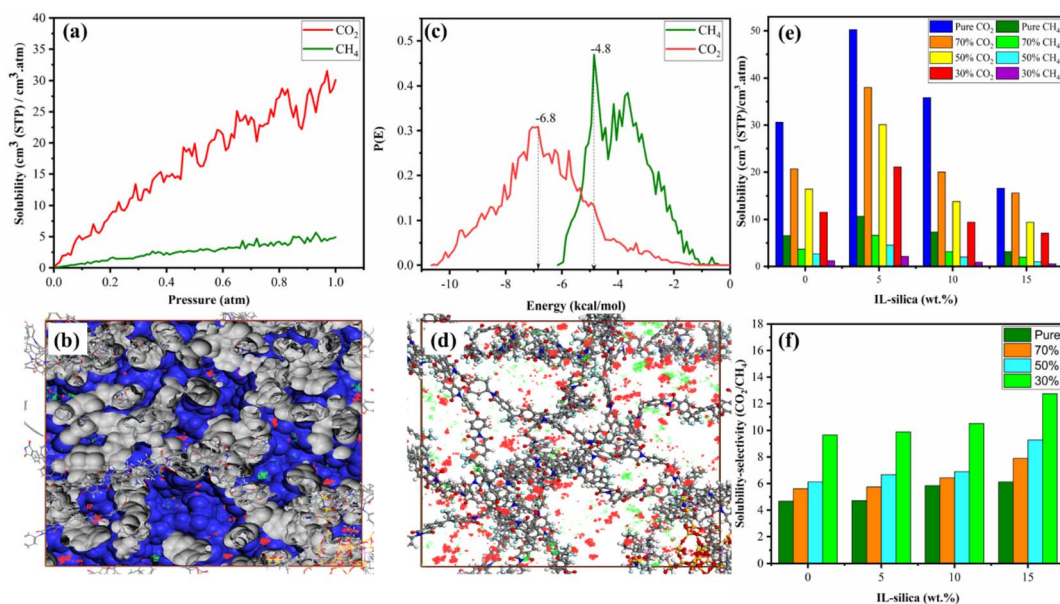


Fig. 9 For 50% CO<sub>2</sub> and 50% CH<sub>4</sub> in 5 wt% IL-silica/6FDA-ODA nanocomposite membrane (a) adsorption isotherm, (b) density distribution at interface, (c) sorption energy distribution, and (d) density distribution of binary gas mixture of CO<sub>2</sub> (red points) and CH<sub>4</sub> (green points) molecules; under different mixed gas concentrations and filler weight percentages (e) CO<sub>2</sub>/CH<sub>4</sub> solubility, (f) CO<sub>2</sub>/CH<sub>4</sub> solubility–selectivity.

ODA polymer increased the solubility of CO<sub>2</sub>. The interfacial adhesion between the polymer and filler was enhanced by ionic liquid modified silica, which also increased the number of polymer–filler pores and enhanced gas solubility. Thus, based on the results obtained in this work, it can be said that the solubility of CO<sub>2</sub> gas in the membrane is increased by adding the ionic liquid modified silica particles. However, the gas solubility decreased as the quantity of IL-silica nanoparticles increased beyond a certain point. For instance, for the 6FDA-ODA/5 wt% IL-silica MMM, the solubility of CO<sub>2</sub> is 50.23 cm<sup>3</sup> (STP) per cm<sup>3</sup> atm, but for the 6FDA-ODA/10 wt% IL-silica MMM, it is reduced to 35.85 cm<sup>3</sup> (STP) per cm<sup>3</sup> atm. This indicates that the solubility decreases with increasing IL-silica content as shown in Fig. 9(e). The decrease in solubility is because of the blockage effect of the ionic liquid, which may act as a potential barrier against the entry of gas molecules, reducing the number of molecules with sufficient energy to pass through and reach to the active sites of the membrane. This behavior was also supported by the fractional free volume which decreased as the weight percentage of IL-silica increased.<sup>112</sup> The solubility selectivity values of gases with different compositions in MMM with varying filler loadings, shown in Fig. 9(f), demonstrate that increase in filler loadings makes MMM more selective. The highest solubility–selectivity was obtained at 15 wt% IL-silica due to confined pore volume that makes MMM more selective, the same effect was also noted in earlier research.<sup>28,113</sup>

**3.2.2 Diffusivity of CO<sub>2</sub>/CH<sub>4</sub>.** Fig. 10(a)–(c) provide a visual representation to demonstrate that the simulation was executed over a duration of 5000 picoseconds in order to establish the distinctiveness of the anomalous region from the Einstein diffusion region for a 5 wt% IL-silica under a 50% CO<sub>2</sub> gas concentration. Following this, the inclination of the Einstein

normal diffusion regime was employed to ascertain the diffusivity. The diffusivity results obtained for mixed gas (50%/50% CO<sub>2</sub>/CH<sub>4</sub>) in 6FDA-ODA under similar conditions (at 35 °C, 10 atm,  $2.28 \times 10^{-8}$ ,  $0.263 \times 10^{-8}$  cm<sup>2</sup> s<sup>-1</sup>) are replicable with the experimental data ( $2.1 \times 10^{-8}$ ,  $0.24 \times 10^{-8}$  cm<sup>2</sup> s<sup>-1</sup>) with 8.6 and 9% error, respectively.<sup>114</sup>

The membrane's pores are precisely sized in relation to the gas molecule's kinetic (sieving) diameter. Due to this, smaller gases can now diffuse far more quickly than molecules of bigger gases. In this case, the CO<sub>2</sub> has smaller kinetic diameter (3.3 Å) than CH<sub>4</sub> (3.8 Å) causing separation of CO<sub>2</sub>/CH<sub>4</sub> gases.<sup>115</sup> One could assume that CH<sub>4</sub> is unable to enter the tiny pores because CH<sub>4</sub> has substantially larger diameter. Even the more open pores, where CO<sub>2</sub> diffuses more freely, are practically impossible for the larger CH<sub>4</sub> molecule to pass through.<sup>115</sup> As the fractions of IL-silica in the membranes increased to 5 wt%, there was an observed increase in the diffusion coefficients of the gases. This phenomenon can be attributed to the disruption of the polymer chains caused by IL-silica nanoparticles, resulting in the creation of voids in the configuration of the 6FDA-ODA.<sup>28</sup> For greater weight proportions of IL-silica, the diffusivity of penetrant gases exhibited a decline; however, the selectivity of diffusivity demonstrated an enhancement. This phenomenon can be attributed to the pore occupancy either by polymer chains or by ionic liquid, resulting in a diminished pathway for the transportation of gas molecules.<sup>31</sup> The existence of filler nanoparticles within the polymer phase generally produces a physical barrier within the membrane, rendering the permeation of gas molecules challenging.<sup>116</sup> It was observed that the diffusivity of CO<sub>2</sub> was higher than that of CH<sub>4</sub> in all the structures, this can be attributed to smaller kinetic diameter of CO<sub>2</sub> as compared to CH<sub>4</sub>.<sup>117</sup> The dissimilarity in size between the penetrants and their respective diffusing capacities resulted in



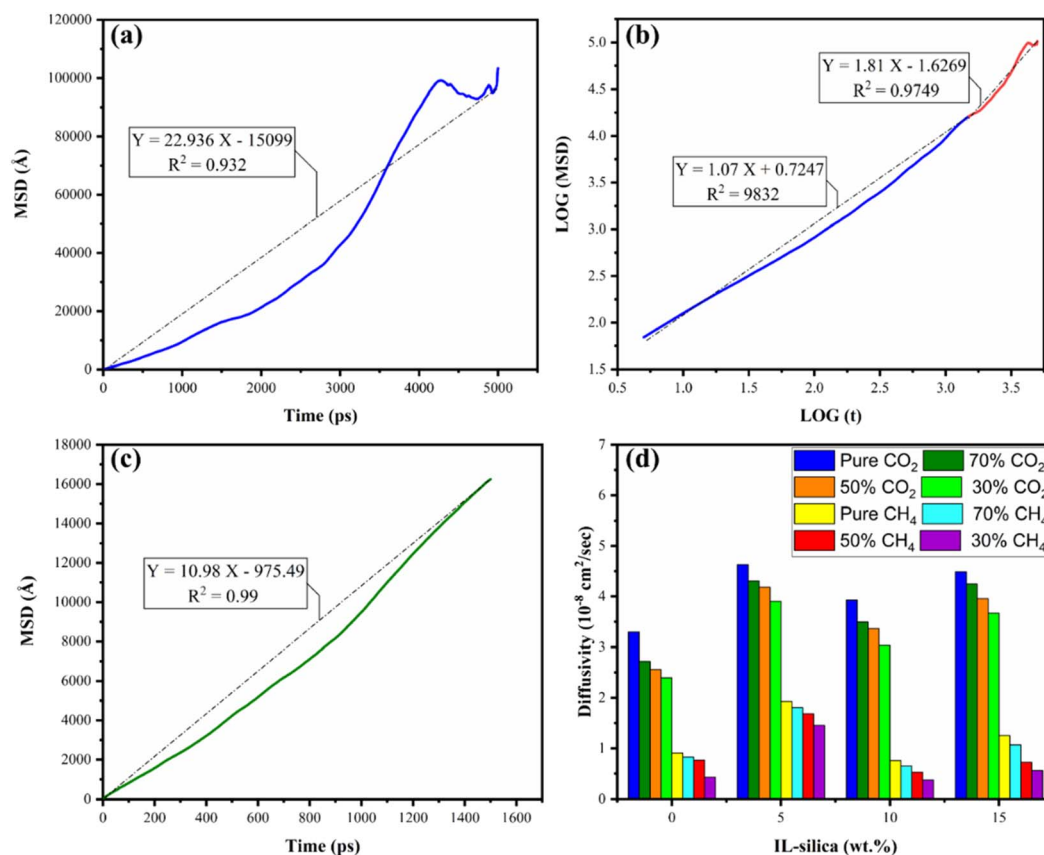


Fig. 10 (a) Mean square displacement (MSD), (b) logarithmic plot for determination of Einstein diffusion region, (c) normal region plot for evaluation of diffusivity coefficients, and (d) diffusion coefficients of CO<sub>2</sub>/CH<sub>4</sub> in IL-silica/6FDA-ODA MMM with varying mixed gas concentrations and different filler weight percentage.

the enhanced diffusivity of CO<sub>2</sub> gas molecules than CH<sub>4</sub> molecules.<sup>118</sup> The presence of ionic liquid, possessing a higher affinity for CO<sub>2</sub> molecules in comparison to CH<sub>4</sub>, can be an additional contributing factor to the notable augmentation in the diffusion of CO<sub>2</sub> gas molecules.<sup>119–121</sup> In general, the strong affinity between CO<sub>2</sub> molecules and the ionic liquid can lead to the formation of transient complexes or enhanced solvation states. These interactions can facilitate the movement of CO<sub>2</sub> through the membrane matrix by reducing the energy barrier for diffusion. Additionally, the higher affinity leads to a greater local concentration of CO<sub>2</sub> molecules, which forms augmented concentration gradient as a driving force for diffusion to occur within the membrane matrix. Overall, the enhancement of weight percentages of silica modified with ionic liquid across diverse gas concentrations led to an improvement in both diffusion and diffusion selectivity.

**3.2.3 Permeability and permselectivity in IL-silica/6FDA-ODA based MMMs.** The permeability and selectivity of the simulated structure was calculated using eqn (12) and (13) and the results are shown in Fig. 11. Fig. 11 presents the permeabilities of CO<sub>2</sub> and CH<sub>4</sub>, as well as the permeability selectivity for ionic liquid decorated silica/6FDA-ODA MMMs. Additionally, it depicts the position of the gas permeability data of IL-

silica/6FDA-ODA MMMs with reference to the Robeson upper bounds.<sup>122–124</sup>

As can be seen from Fig. 11, CO<sub>2</sub> exhibits a higher level of permeability compared to CH<sub>4</sub> owing to its higher diffusivity due to smaller size and greater condensability, as signified by its critical temperature ( $T_c$ ), for instance,  $T_{c,CO_2} = 304$  K,  $T_{c,CH_4} = 191$  K,<sup>125</sup> indicating CO<sub>2</sub> is more soluble than that of the CH<sub>4</sub>. As mentioned in section 3.2.2, the increased condensability also further results in a higher local concentration of CO<sub>2</sub> molecules, thereby enhancing the concentration gradient that drives diffusion within the membrane matrix.<sup>126</sup> The permeability of gas molecules increased to 89% with an increasing 5 wt% filler as compared to pure polymer. A reduction in permeability was noticed for a higher weight percentage (10 and 15 wt%) of modified filler. The subsequent factors may contribute to the observed reduction in permeability. (1) As previously mentioned, 6FDA-ODA exhibits a significant degree of gas permeability, particularly towards CO<sub>2</sub>. Consequently, the incorporation of fillers with lesser permeability would result in reduced gas permeabilities throughout the MMMs. (2) The clustering of the alkyl chains of ionic liquid supported on silica surface with the 6FDA-ODA layer. (3) The inclusion of filler in the polymeric matrix causes a larger tortuosity, which disrupts gas diffusion and lengthens the pathlength through the

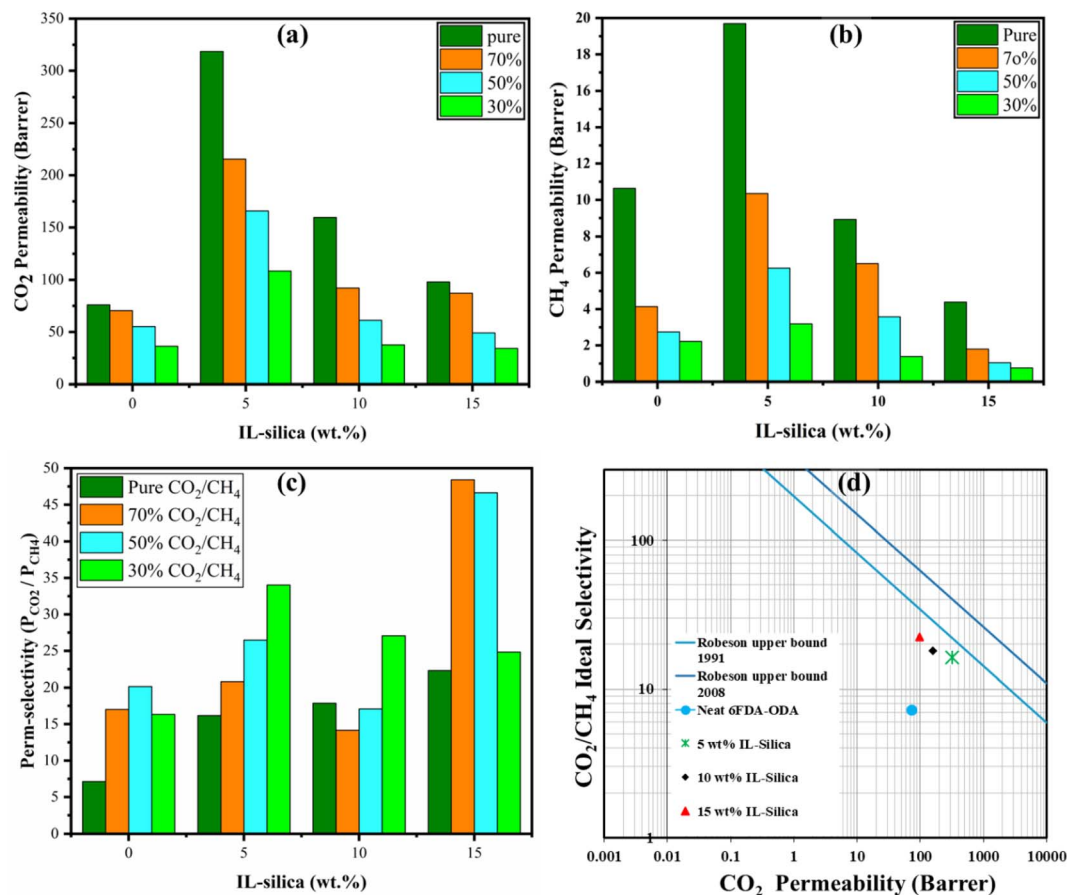


Fig. 11 Transport properties under different gas composition in a membrane with varying filler loadings (a) CO<sub>2</sub> gas permeability, (b) CH<sub>4</sub> gas permeability, (c) CO<sub>2</sub>/CH<sub>4</sub> permeability–selectivity; (d) membrane performance as compared with Robeson upper bounds.

MMMs.<sup>127</sup> (4) The mobility of penetrant gas molecules is hampered by polymer rigidification adjacent to the porous particles.<sup>128</sup> (5) The filler's pores may get smaller due to pore blockage by the polymer chains or alkyl chains of IL which may result a choked gas flow.<sup>129</sup> (6) A completely blocked set of pores due to heavily adsorbed gas molecules results in a jammed sieve.<sup>130</sup>

Based on the obtained results it can be said that utilizing smaller amounts of inorganic fillers is a better choice in gas separation in mixed matrix membranes (MMMs). Earlier studies have also experienced a similar effect.<sup>29,30,39</sup> Nonetheless, regardless of the noticed clustering, the permeability values of 10 wt% IL-silica for pure gas conditions still remained greater than those for the pure 6FDA-ODA polymer. Under identical conditions, the permeability values for pure gases are greater than that of the gases in mixed condition, depending on the solubility and diffusivity coefficients. The gas permeability in mixed gas decreased as the concentration of that gas decreased can be attributed to the occurrence of the competitive gas transport within the membrane.

The CO<sub>2</sub>/CH<sub>4</sub> selectivity was observed to be correlated with the membrane physical properties through inclusion of IL-silica, typically with respect to the effect of free volume and cavity size distribution.<sup>131</sup> At higher loadings, reduced fractional free volume but increasing *d*-spacing was observed, implying

the number of voids was reduced but created at bigger size due to agglomeration.<sup>132,133</sup> At 15 wt% IL-silica, void size effect was dominant at higher CO<sub>2</sub> concentrations, which contributed to an increment in the CO<sub>2</sub>/CH<sub>4</sub> selectivity, as seen from Fig. 11(c). At higher concentrations of CO<sub>2</sub> (70% and 50%), the increase in the number of CO<sub>2</sub> molecules enhanced the interaction with the voids within the membrane, which facilitated the selective transport of CO<sub>2</sub> over CH<sub>4</sub>. In contrast, the membrane's permeability towards CH<sub>4</sub> was decreased *via* competitive transport, resulting in enhanced selectivity ultimately.<sup>126</sup> On the other hand, for reduced CO<sub>2</sub> concentration at 30%, there was a reduced driving force for entrance of CO<sub>2</sub> within the limited number of microvoids, which further decreased its transport performance. Additionally, the ionic liquid at higher loading could potentially serve as a barrier due to its blocking effect,<sup>134,135</sup> effectively reducing the number of gas molecules with sufficient energy to penetrate and reach the active sites of the membrane that reduced gas permeability, typically at low concentration with reduced driving force. The decrease in CO<sub>2</sub> gas permeability will ultimately result in a decrease in gas permeability-selectivity.<sup>136</sup>

The highest permeability and selectivity were observed at 5 wt% and 15 wt%, respectively. It became evident that the addition of IL-silica nanoparticles to the membrane enhanced the characteristics of the membrane as well as the solubility of

Table 3 Comparing CO<sub>2</sub> separation efficiency of IL@filler/polymer based MMMs

| Membrane                                   | Filler (wt%) | Operating conditions |           | $P_{\text{CO}_2}$ (barrer) | Selectivity ( $P_{\text{CO}_2}/P_{\text{CH}_4}$ ) | References |
|--|--------------|----------------------|-----------|----------------------------|---|------------|
|  |              | $T$ (°C)             | $P$ (bar) |                            |   |            |
| [Emim][Tf <sub>2</sub> N]@silica/PC        | 3            | 25                   | 2         | 34.6 GPU                   | 86.5  | 106        |
| NH <sub>2</sub> @silica/PSF                | 20           | 35                   | 1         | 62                         | 11  | 30         |
| [Emim][Tf <sub>2</sub> N]@SAPO-34/PSF      | 5            | 25                   | 3.75      | 7.24 GPU                   | 20.3  | 23         |
| [APTMS][AC]@ZIF-67/PSF                     | 30           | 25                   | 10        | 20.12                      | 67  | 145        |
| [Bmim][Tf <sub>2</sub> N]@ZIF-8/Pebax1657  | 15           | 25                   | 1         | 104                        | 34.8  | 22         |
| [APTMS][AC]@zeolite 4A/PSF                 | 30           | 25                   | 10        | 16                         | 30  | 21         |
| PAMAM@CTS/PSF                              | 10           | 40                   | 1         | 61 GPU                     | —   | 146        |
| [BMIM][PF <sub>6</sub> ]@ZIF-8/PEBAX       | 25           | 40                   | 1         | 117                        | 84.5  | 147        |
| [P8883][Tf <sub>2</sub> N]@silica/6FDA-ODA | 5            | 40                   | 1         | 319                        | 16.2  | This work  |

gases. This enhancement demonstrated that when combined with the 6FDA-ODA polymer, the IL decorated silica nanoparticles may be able to address the flaws in the inter-crystalline structure of the membrane surface. Furthermore, the presence of an ionic liquid improved the dispersion of the nanofillers on the membrane surface, improved polymer–filler compatibility and exhibited a strong affinity for CO<sub>2</sub> due to the prevalence of an anionic group of the ionic liquid. Due to the complex pathways that impose restrictions on the transportation of CH<sub>4</sub>, the combined effects of the interaction between polymer and ionic liquid modified filler result in a selective transport mechanism that effectively limits the loss of CH<sub>4</sub>.<sup>137–140</sup> Compared to the pristine polymeric membrane, the increase in permeability and selectivity for 15 wt% ionic liquid modified filler based MMMs was found to be 22% and 68%, respectively for pure gas condition. The gas permeability and selectivity of the pristine 6FDA-ODA polymer and the IL-silica MMMs were compared to the upper bounds set by Robeson.<sup>30,141–143</sup> Fig. 11(d) illustrates that the IL-silica/6FDA-ODA based MMMs exhibited significantly greater permeability and selectivity compared to the pristine 6FDA-ODA membrane and were found to be in closer proximity to the Robeson plot.

**3.2.4 Comparison of optimized MMM with previously studied MMMs.** A comparison was conducted to assess the performance of the IL-silica/6FDA-ODA based MMMs in the context of CO<sub>2</sub>/CH<sub>4</sub> separation. This benchmarking exercise involved a review of relevant literature (*i.e.*, IL@filler/polymer), the findings of which are presented in Table 3. For example, an MMM composite was created by incorporating 30 wt% of [APTMS][AC]@zeolite-4A into PSF. The MMM exhibited CO<sub>2</sub> permeability of 16 barrer and CO<sub>2</sub>/CH<sub>4</sub> selectivity of 30.<sup>29</sup> The [BMIM][Tf<sub>2</sub>N]/ZIF/Pebax mixed matrix membrane with 15 wt% IL-filler exhibited a CO<sub>2</sub> permeability of 104 barrer and a CO<sub>2</sub>/CH<sub>4</sub> selectivity of 34. The [P8883][Tf<sub>2</sub>N]-silica/6FDA-ODA with 5 wt% IL-silica demonstrated a 20-fold increase in CO<sub>2</sub> permeability (319 barrer) and a 1.85-fold decrease in CO<sub>2</sub>/CH<sub>4</sub> selectivity (16.2) compared to the [BMIM][Tf<sub>2</sub>N]/ZIF/Pebax MMM. There was no notable difference in CO<sub>2</sub>/CH<sub>4</sub> selectivities between the two materials.<sup>21</sup> The outcomes regarding the gas mixture of CO<sub>2</sub>/CH<sub>4</sub> demonstrate that the presence of [P8883][Tf<sub>2</sub>N] supported on silica enhances the permeability of CO<sub>2</sub> in

the membrane. This enhancement can be attributed to the presence of [Tf<sub>2</sub>N] ions,<sup>144</sup> which are CO<sub>2</sub> philic groups, as well as the longer alkyl chain on the cation, which slightly increases the solubility. Furthermore, the combination of these groups and the molecular sieving ability of the MMM leads to an improved permeability with a satisfactorily selective nature.

The permeability and selectivity of the [P8883][Tf<sub>2</sub>N]-silica/6FDA-ODA based MMM in this investigation, particularly with 5 wt% IL-silica loading, surpasses all previously reported literature results, as shown in Table 3. The permeability and selectivity data presented here indicate enhanced CO<sub>2</sub> permeability and CO<sub>2</sub>/CH<sub>4</sub> selectivity, showcasing the potential of integrating phosphonium-based IL-silica filler in polymers to create IL-silica/polymer MMMs. In general, the present study aimed to enhance the gas permeability of CO<sub>2</sub> and the selectivity of CO<sub>2</sub>/CH<sub>4</sub> by utilizing a silica substrate decorated with an IL. This innovative design successfully addressed the common tradeoff problem encountered in gas separation membranes. The improved CO<sub>2</sub> permeability and selectivity have the potential to be applied in offshore separation processes with high levels of contaminants. This would lead to increased flux while minimizing the required membrane area in confined locations.

## 4 Conclusion

In conclusion, MMM consisting of a gas-selective silica modified with [P8883][Tf<sub>2</sub>N] IL (IL-silica) filler, and 6FDA-ODA polymer, has been effectively designed and simulated. The *NPT* ensemble, energetic based cavity-sizing algorithm, grand canonical Monte Carlo (GCMC) and molecular dynamics (MD) simulation techniques using the COMPASS force field with 500 ps simulation time were performed to calculate the density and glass transition temperature, fractional free volume, diffusivity, and solubility respectively. The impact of IL-filler loading and feed gas concentration on the performance of the MMM has been examined. The results demonstrated that the incorporation of IL-silica led to a reduction in inter-crystallinity and free volume of the structure with improved  $T_g$  value, resulting in a more stable and selective gas separation process. The modification of the filler with IL has significantly enhanced the separation performance of membrane. By incorporating 5 wt%

IL-silica, the IL-silica/6FDA-ODA MMM has demonstrated an approximate 80% improvement in permeability and a 56% improvement in selectivity. The observed enhancement can be ascribed to the improved interfacial compatibility between the polymer and filler at the interface, enhanced dispersion of the ionic liquid-modified filler within the polymer, and increased carbon dioxide attraction with the ionic liquid. Using molecular simulation, this study highlights the potential for supporting IL into silica *via* a straightforward grafting technique to construct MMM with acceptable separation performance. The results obtained from the model's validation indicated a satisfactory level of precision in predicting the permeability of CO<sub>2</sub> and CH<sub>4</sub>. The mean percentage error, when compared to experimental results, was found to be less than 10%. This article describes the techniques to improve the filler and polymer's performance and emphasizes the benefits of using molecular simulation to ascertain the features of gas permeation in order to further evaluate the correlation's applicability. This approach offers the benefits of reduced error, time commitment, and cost-effectiveness, which can be valuable in material screening and the optimization of process conditions to enhance the separation performance of the membrane. Furthermore, this concept can be extended to optimize other factors that influence the physical properties and performance of IL-modified silica-based MMMs, such as IL selection, temperature, and pressure variations.

## Author contributions

Mehtab Ali Darban: writing original manuscript, software, formal analysis. Serene Sow Mun Lock: supervision, formal analysis, writing – review & editing. Suhaib Umer Ilyas: visualization, investigation. Dun-Yen Kang: writing – review & editing. Mohd Hafiz Dzarfan Othman: writing – review & editing. Chung Loong Yiin: resources; writing – review & editing. Sharjeel Waqas: writing – review & editing. Zunara Bashir: writing – review & editing.

## Conflicts of interest

The authors assert that they do not possess any recognized conflicting financial concerns or personal bonds that may have seemed to affect the research presented in this manuscript.

## Acknowledgements

We want to acknowledge the financial support provided by the Ministry of Higher Education, Malaysia, under Fundamental Research Grant Scheme (FRGS) (Ref. No. FRGS/1/2022/TK09/UTP/03/3, Cost Centre: 015MA0-153), The Murata Science Foundation (Grant No. 23MP07, Cost Centre: 015ME0-351) and YUTP-Fundamental Research Grant (Cost Centre: 015LCO-498). Moreover, we would also like to acknowledge the technical support from the Institute of Sustainable Energy and Resources, Centre of Carbon Capture, Utilisation and Storage (CCCUS).

## References

- 1 M. Nawaz, H. Suleman and A. S. Maulud, Carbon Capture and Utilization: A Bibliometric Analysis from 2007–2021, *Energies*, 2022, **15**(18), 1–17, DOI: [10.3390/en15186611](https://doi.org/10.3390/en15186611).
- 2 H. Lotfali nejad, M. R. Ghasemi, A. H. Nazemi, *et al.*, Continuous adsorption process of CO<sub>2</sub>/N<sub>2</sub>/H<sub>2</sub>O from CH<sub>4</sub> flow using type A zeolite adsorbents in the presence of ultrasonic waves, *Results Eng.*, 2023, **20**, 101490, DOI: [10.1016/j.rineng.2023.101490](https://doi.org/10.1016/j.rineng.2023.101490).
- 3 A. A. Abdulabbas, T. J. Mohammed and T. A. Al-Hattab, Parameters estimation of fabricated polysulfone membrane for CO<sub>2</sub>/CH<sub>4</sub> separation, *Results Eng.*, 2024, 101929, DOI: [10.1016/j.rineng.2024.101929](https://doi.org/10.1016/j.rineng.2024.101929).
- 4 M. Balçık, S. B. Tantekin-Ersolmaz, I. Pinnau, *et al.*, CO<sub>2</sub>/CH<sub>4</sub> mixed-gas separation in PIM-1 at high pressures: bridging atomistic simulations with process modeling, *J. Membr. Sci.*, 2021, **640**, 119838, DOI: [10.1016/J.MEMSCI.2021.119838](https://doi.org/10.1016/J.MEMSCI.2021.119838).
- 5 A. F. Yazid, H. Mukhtar, R. Nasir, *et al.*, Incorporating carbon nanotubes in nanocomposite mixed-matrix membranes for gas separation: a review, *Membranes*, 2022, **12**(6), 589, DOI: [10.3390/membranes12060589](https://doi.org/10.3390/membranes12060589).
- 6 D. Huang, Q. Xin, Y. Ni, *et al.*, Synergistic effects of zeolite imidazole framework@graphene oxide composites in humidified mixed matrix membranes on CO<sub>2</sub> separation, *RSC Adv.*, 2018, **8**(11), 6099–6109, DOI: [10.1039/c7ra09794h](https://doi.org/10.1039/c7ra09794h).
- 7 T. D. Shittu and O. B. Ayodele, Experimental and computational investigation of CO<sub>2</sub>–CH<sub>4</sub> reforming to syngas over zeolite A supported oxalate ligands functionalized Ni catalysts, *Results Eng.*, 2022, **16**, 100630, DOI: [10.1016/j.rineng.2022.100630](https://doi.org/10.1016/j.rineng.2022.100630).
- 8 S. K. Singh and A. W. Savoy, Ionic Liquids Synthesis and Applications: An Overview, *J. Mol. Liq.*, 2020, **297**, 112038, DOI: [10.1016/j.molliq.2019.112038](https://doi.org/10.1016/j.molliq.2019.112038).
- 9 V. O. Viola, T. F. de Aquino, S. T. Estevam, *et al.*, Synthesis and application of two types of amine sorbents impregnated on silica from coal fly ash for CO<sub>2</sub> capture, *Results Eng.*, 2023, **20**, 101596, DOI: [10.1016/j.rineng.2023.101596](https://doi.org/10.1016/j.rineng.2023.101596).
- 10 M. Chowdhury, P. Poddar, A. S. M. Kashem, *et al.*, Surface modification of polycarbonate films with 2-hydroxyethylmethacrylate (HEMA) and N-vinyl pyrrolidone (NVP) monomers by radiation techniques, *Results Eng.*, 2024, **22**, 101981, DOI: [10.1016/j.rineng.2024.101981](https://doi.org/10.1016/j.rineng.2024.101981).
- 11 O. A. Odunlami, D. A. Vershima, T. E. Oladimeji, *et al.*, Advanced Techniques for the Capturing and Separation of CO<sub>2</sub> – A Review, *Results Eng.*, 2022, **1**, 100512, DOI: [10.1016/j.rineng.2022.100512](https://doi.org/10.1016/j.rineng.2022.100512).
- 12 F. L. Bernard, E. A. Duarte, B. B. Polesso, *et al.*, CO<sub>2</sub> sorption using encapsulated imidazolium-based fluorinated ionic liquids, *Environ. Challenges*, 2021, **4**, 100109, DOI: [10.1016/j.envc.2021.100109](https://doi.org/10.1016/j.envc.2021.100109).
- 13 Z. J. Li, M. Y. Zhen, Q. Q. Xu, *et al.*, Preparing supported ionic liquids by continuous supercritical carbon dioxide adsorption method, *Mater. Res. Express*, 2019, **6**(8), 112038, DOI: [10.1088/2053-1591/ab1d41](https://doi.org/10.1088/2053-1591/ab1d41).



- 14 Y. C. Hudiono, T. K. Carlisle, J. E. Bara, *et al.*, A three-component mixed-matrix membrane with enhanced CO<sub>2</sub> separation properties based on zeolites and ionic liquid materials, *J. Membr. Sci.*, 2010, **350**(1–2), 117–123, DOI: [10.1016/j.memsci.2009.12.018](https://doi.org/10.1016/j.memsci.2009.12.018).
- 15 J. Zhu, B. He, J. Huang, *et al.*, Effect of immobilization methods and the pore structure on CO<sub>2</sub> separation performance in silica-supported ionic liquids, *Microporous Mesoporous Mater.*, 2018, **260**(September 2017), 190–200, DOI: [10.1016/j.micromeso.2017.10.035](https://doi.org/10.1016/j.micromeso.2017.10.035).
- 16 J. Xu, H. Jia, N. Yang, *et al.*, High efficiency gas permeability membranes from ethyl cellulose grafted with ionic liquids, *Polymers*, 2019, **11**(11), 1900, DOI: [10.3390/polym11111900](https://doi.org/10.3390/polym11111900).
- 17 A. S. Aquino, F. L. Bernard, J. V. Borges, *et al.*, Rationalizing the role of the anion in CO<sub>2</sub> capture and conversion using imidazolium-based ionic liquid modified mesoporous silica, *RSC Adv.*, 2015, **5**(79), 64220–64227, DOI: [10.1039/c5ra07561k](https://doi.org/10.1039/c5ra07561k).
- 18 Y. Wang and R. T. Yang, Template Removal from SBA-15 by Ionic Liquid for Amine Grafting: Applications to CO<sub>2</sub> Capture and Natural Gas Desulfurization, *ACS Sustain. Chem. Eng.*, 2020, **8**(22), 8295–8304, DOI: [10.1021/acssuschemeng.0c01941](https://doi.org/10.1021/acssuschemeng.0c01941).
- 19 V. Hiremath, A. H. Jadhav, H. Lee, *et al.*, Highly reversible CO<sub>2</sub> capture using amino acid functionalized ionic liquids immobilized on mesoporous silica, *Chem. Eng. J.*, 2016, **287**, 602–617, DOI: [10.1016/j.cej.2015.11.075](https://doi.org/10.1016/j.cej.2015.11.075).
- 20 M. Bahadori, A. Marandi, S. Tangestaninejad, *et al.*, Ionic Liquid-Decorated MIL-101(Cr) via Covalent and Coordination Bonds for Efficient Solvent-Free CO<sub>2</sub> Conversion and CO<sub>2</sub> Capture at Low Pressure, *J. Phys. Chem. C*, 2020, **124**(16), 8716–8725, DOI: [10.1021/acs.jpcc.9b11668](https://doi.org/10.1021/acs.jpcc.9b11668).
- 21 A. Ilyas, N. Muhammad, M. A. Gilani, *et al.*, Effect of zeolite surface modification with ionic liquid [APTMS][Ac] on gas separation performance of mixed matrix membranes, *Sep. Purif. Technol.*, 2018, **205**, 176–183, DOI: [10.1016/j.seppur.2018.05.040](https://doi.org/10.1016/j.seppur.2018.05.040).
- 22 H. Li, L. Tuo, K. Yang, *et al.*, Simultaneous enhancement of mechanical properties and CO<sub>2</sub> selectivity of ZIF-8 mixed matrix membranes: Interfacial toughening effect of ionic liquid, *J. Membr. Sci.*, 2016, **511**, 130–142, DOI: [10.1016/j.memsci.2016.03.050](https://doi.org/10.1016/j.memsci.2016.03.050).
- 23 N. N. R. Ahmad, C. P. Leo, A. W. Mohammad, *et al.*, Modification of gas selective SAPO zeolites using imidazolium ionic liquid to develop polysulfone mixed matrix membrane for CO<sub>2</sub> gas separation, *Microporous Mesoporous Mater.*, 2017, **244**, 21–30, DOI: [10.1016/j.micromeso.2016.10.001](https://doi.org/10.1016/j.micromeso.2016.10.001).
- 24 G. Liu, A. Cadiou, Y. Liu, *et al.*, Enabling Fluorinated MOF-Based Membranes for Simultaneous Removal of H<sub>2</sub>S and CO<sub>2</sub> from Natural Gas, *Angew. Chem., Int. Ed.*, 2018, **57**(45), 14811–14816, DOI: [10.1002/anie.201808991](https://doi.org/10.1002/anie.201808991).
- 25 N. E. Hira, S. S. M. Lock, U. Arshad, *et al.*, Screening of Metal Oxides and Hydroxides for Arsenic Removal from Water Using Molecular Dynamics Simulations, *ACS Omega*, 2023, **8**(50), 48130–48144, DOI: [10.1021/acsomega.3c07014](https://doi.org/10.1021/acsomega.3c07014).
- 26 Y. Numazawa, Y. Matsukawa, Y. Hara, *et al.*, Large-scale simulation of CO<sub>2</sub> gasification reaction with mass transfer for metallurgical coke: Comparison with lab-scale experiment at 1373 K in early stage, *Results Eng.*, 2023, **19**, 101212, DOI: [10.1016/j.rineng.2023.101212](https://doi.org/10.1016/j.rineng.2023.101212).
- 27 S. Velioglu, M. G. Ahunbay and S. B. Tantekin-Ersolmaz, Investigation of CO<sub>2</sub>-induced plasticization in fluorinated polyimide membranes via molecular simulation, *J. Membr. Sci.*, 2012, **417–418**, 217–227, DOI: [10.1016/j.memsci.2012.06.043](https://doi.org/10.1016/j.memsci.2012.06.043).
- 28 K. Golzar, S. Amjad-Iranagh, M. Amani, *et al.*, Molecular simulation study of penetrant gas transport properties into the pure and nanosized silica particles filled polysulfone membranes, *J. Membr. Sci.*, 2014, **451**, 117–134, DOI: [10.1016/j.memsci.2013.09.056](https://doi.org/10.1016/j.memsci.2013.09.056).
- 29 K. Asif, S. S. M. Lock, S. A. A. Taqvi, *et al.*, A molecular simulation study of silica/polysulfone mixed matrix membrane for mixed gas separation, *Polymers*, 2021, **13**(13), 2199, DOI: [10.3390/polym13132199](https://doi.org/10.3390/polym13132199).
- 30 K. Asif, S. S. M. Lock, S. A. A. Taqvi, *et al.*, A molecular simulation study on amine-functionalized silica/polysulfone mixed matrix membrane for mixed gas separation, *Chemosphere*, 2023, **311**(October 2022), 136936, DOI: [10.1016/j.chemosphere.2022.136936](https://doi.org/10.1016/j.chemosphere.2022.136936).
- 31 Y. Ban, Z. Li, Y. Li, *et al.*, Confinement of Ionic Liquids in Nanocages: Tailoring the Molecular Sieving Properties of ZIF-8 for Membrane-Based CO<sub>2</sub> Capture, *Angew. Chem.*, 2015, **54**(51), 15483–15487, DOI: [10.1002/ange.201505508](https://doi.org/10.1002/ange.201505508).
- 32 F. W. Harris, Synthesis of aromatic polyimides from dianhydrides and diamines, *Polyimides*, 1990, 1–37, DOI: [10.1007/978-94-010-9661-4\\_1](https://doi.org/10.1007/978-94-010-9661-4_1).
- 33 J. Ren, L. Wu and B. G. Li, Preparation and CO<sub>2</sub> sorption/desorption of N-(3-aminopropyl)aminoethyl tributylphosphonium amino acid salt ionic liquids supported into porous silica particles, *Ind. Eng. Chem. Res.*, 2012, **51**(23), 7901–7909, DOI: [10.1021/ie2028415](https://doi.org/10.1021/ie2028415).
- 34 N. N. R. Ahmad, C. P. Leo, A. W. Mohammad, *et al.*, Recent progress in the development of ionic liquid-based mixed matrix membrane for CO<sub>2</sub> separation: a review, *Int. J. Energy Res.*, 2021, **45**(7), 9800–9830, DOI: [10.1002/er.6518](https://doi.org/10.1002/er.6518).
- 35 K. J. Fraser and D. R. MacFarlane, Phosphonium-based ionic liquids: An overview, *Aust. J. Chem.*, 2009, **62**(4), 309–321, DOI: [10.1071/CH08558](https://doi.org/10.1071/CH08558).
- 36 W. A. Henderson Jr and S. A. Buckner, The Nucleophilicity of Phosphines, *J. Am. Chem. Soc.*, 2019, **82**(22), 5794–5800, DOI: [10.1021/ja01507a009](https://doi.org/10.1021/ja01507a009).
- 37 K. R. Seddon, A. Stark and M. J. Torres, Viscosity and density of 1-alkyl-3-methylimidazolium ionic liquids, *ACS Symp. Ser.*, 2002, **819**, 34–49, DOI: [10.1021/bk-2002-0819.ch004](https://doi.org/10.1021/bk-2002-0819.ch004).
- 38 S. Zheng, S. Zeng, Y. Li, *et al.*, State of the Art of Ionic Liquid-Modified Adsorbents for CO<sub>2</sub> Capture and Separation, *AIChE J.*, 2022, **68**(2), 17500, DOI: [10.1002/aic.17500](https://doi.org/10.1002/aic.17500).

- 39 K. Golzar, S. Amjad-Iranagh, M. Amani, *et al.*, Molecular simulation study of penetrant gas transport properties into the pure and nanosized silica particles filled polysulfone membranes, *J. Membr. Sci.*, 2014, **451**, 117–134, DOI: [10.1016/j.memsci.2013.09.056](https://doi.org/10.1016/j.memsci.2013.09.056).
- 40 J. Schumacher, D. Meyer, J. Friedland, *et al.*, Evaluation of the application of different diffusion models for the methanation of CO/CO<sub>2</sub> mixtures, *Results Eng.*, 2022, **13**, 100355, DOI: [10.1016/j.rineng.2022.100355](https://doi.org/10.1016/j.rineng.2022.100355).
- 41 D. M. Anstine and C. M. Colina, Sorption-induced polymer rearrangement: approaches from molecular modeling, *Polym. Int.*, 2021, **70**(7), 984–989, DOI: [10.1002/pi.6124](https://doi.org/10.1002/pi.6124).
- 42 S. S. M. Lock, K. K. Lau, A. M. Shariff, *et al.*, Computational insights on the role of film thickness on the physical properties of ultrathin polysulfone membranes, *RSC Adv.*, 2017, **7**(70), 44376–44393, DOI: [10.1039/c7ra07277e](https://doi.org/10.1039/c7ra07277e).
- 43 S. Neyertz and D. Brown, An optimized fully-atomistic procedure to generate glassy polymer films for molecular dynamics simulations, *Comput. Mater. Sci.*, 2020, **174**(December 2019), 109499, DOI: [10.1016/j.commatsci.2019.109499](https://doi.org/10.1016/j.commatsci.2019.109499).
- 44 Q. L. Liu and Y. Huang, Transport behavior of oxygen and nitrogen through organasilicon-containing polystyrenes by molecular simulation, *J. Phys. Chem. B*, 2006, **110**(35), 17375–17382, DOI: [10.1021/jp063174x](https://doi.org/10.1021/jp063174x).
- 45 M. Balçık, S. B. Tantekin-Ersolmaz, I. Pinnau, *et al.*, CO<sub>2</sub>/CH<sub>4</sub> mixed-gas separation in PIM-1 at high pressures: Bridging atomistic simulations with process modeling, *J. Membr. Sci.*, 2021, **640**, 119838, DOI: [10.1016/J.MEMSCI.2021.119838](https://doi.org/10.1016/J.MEMSCI.2021.119838).
- 46 J. Ahn, W. J. Chung, I. Pinnau, *et al.*, Polysulfone/silica nanoparticle mixed-matrix membranes for gas separation, *J. Membr. Sci.*, 2008, **314**(1–2), 123–133, DOI: [10.1016/j.memsci.2008.01.031](https://doi.org/10.1016/j.memsci.2008.01.031).
- 47 J. P. M. Jämbeck and A. P. Lyubartsev, An extension and further validation of an all-atomistic force field for biological membranes, *J. Chem. Theory Comput.*, 2012, **8**(8), 2938–2948, DOI: [10.1021/ct300342n](https://doi.org/10.1021/ct300342n).
- 48 Y. Chen, Q. L. Liu, A. M. Zhu, *et al.*, Molecular simulation of CO<sub>2</sub>/CH<sub>4</sub> permeabilities in polyamide-imide isomers, *J. Membr. Sci.*, 2010, **348**(1–2), 204–212, DOI: [10.1016/j.memsci.2009.11.002](https://doi.org/10.1016/j.memsci.2009.11.002).
- 49 Q. Zheng, Q. Xue, K. Yan, *et al.*, Investigation of molecular interactions between SWNT and polyethylene/polypropylene/polystyrene/polyaniline molecules, *J. Phys. Chem. C*, 2007, **111**(12), 4628–4635, DOI: [10.1021/jp066077c](https://doi.org/10.1021/jp066077c).
- 50 S. J. Lue, T. H. Yang, K. S. Chang, *et al.*, Water diffusivity suppression and ethanol-over-water diffusion selectivity enhancement for ethanol/water mixtures in polydimethylsiloxane-zeolite membranes, *J. Membr. Sci.*, 2012, **635**–**643**, DOI: [10.1016/j.memsci.2012.05.044](https://doi.org/10.1016/j.memsci.2012.05.044).
- 51 O. Hölck, M. Böhning, M. Heuchel, *et al.*, Gas sorption isotherms in swelling glassy polymers-Detailed atomistic simulations, *J. Membr. Sci.*, 2013, **428**, 523–532, DOI: [10.1016/j.memsci.2012.10.023](https://doi.org/10.1016/j.memsci.2012.10.023).
- 52 H. Sun, COMPASS: An Ab Initio Force-Field Optimized for Condensed-Phase Applications-Overview with Details on Alkane and Benzene Compounds, *J. Phys. Chem.*, 1998, **102**, 7338–7364, DOI: [10.1021/jp980939v](https://doi.org/10.1021/jp980939v).
- 53 G. D. Smith, R. L. Jaffe and D. Y. Yoon, Force Field for Simulations of 1,2-Dimethoxyethane and Poly(Oxyethylene) Based upon Ab Initio Electronic Structure Calculations on Model Molecules, *J. Phys. Chem.*, 1993, **97**(49), 12752–12759, DOI: [10.1021/j100151a021](https://doi.org/10.1021/j100151a021).
- 54 G. D. Smith and W. Paul, United Atom Force Field for Molecular Dynamics Simulations of 1,4-Polybutadiene Based on Quantum Chemistry Calculations on Model Molecules, *J. Am. Chem. Soc.*, 1998, **102**(7), 1200–1208, DOI: [10.1021/jp9730858](https://doi.org/10.1021/jp9730858).
- 55 A. T. Hagler, S. Lifson and P. Dauber, Consistent Force Field Studies of Intermolecular Forces in Hydrogen-Bonded Crystals. 2. A Benchmark for the Objective Comparison of Alternative Force Fields, *J. Am. Chem. Soc.*, 1979, **101**(18), 5122–5130, DOI: [10.1021/ja00512a002](https://doi.org/10.1021/ja00512a002).
- 56 H. Sun, S. J. Mumby, J. R. Maple, *et al.*, An Ab Initio CFF93 All-Atom Force Field for Polycarbonates, *J. Am. Chem. Soc.*, 1994, **116**(7), 2918–2981, DOI: [10.1021/ja00086a030](https://doi.org/10.1021/ja00086a030).
- 57 H. Sun, P. Ren and J. R. Fried, The COMPASS Force Field: Parameterization and Validation for Phosphazenes, *Comput. Theor. Polym. Sci.*, 1998, **8**(1–2), 229–246, DOI: [10.1016/S1089-3156\(98\)00042-7](https://doi.org/10.1016/S1089-3156(98)00042-7).
- 58 S. H. Jeong, S. Cho, T. Y. Ha, *et al.*, Structural and dynamical characteristics of short-chain branched ring polymer melts at interface under shear flow, *Polymers*, 2020, **12**(12), 3068, DOI: [10.3390/polym12123068](https://doi.org/10.3390/polym12123068).
- 59 H. Rachapudy, G. G. Smith, V. R. Raju, *et al.*, Properties of Amorphous and Crystallizable Hydrocarbon Polymers. III. Studies of the Hydrogenation of Polybutadiene, *J. Polym. Sci., Polym. Phys. Ed.*, 1979, **17**(7), 1211–1222, DOI: [10.1002/pol.1979.180170706](https://doi.org/10.1002/pol.1979.180170706).
- 60 M. Levitt and S. Lifson, Refinement of Protein Conformations Using a Macromolecular Energy Minimization Procedure, *J. Mol. Biol.*, 1969, **46**(2), 269–278, DOI: [10.1016/0022-2836\(69\)90421-5](https://doi.org/10.1016/0022-2836(69)90421-5).
- 61 R. Fletcher and C. M. Reeves, Function minimization by conjugate gradients, *Comput. J.*, 1964, **7**(2), 149–154, DOI: [10.1093/comjnl/7.2.149](https://doi.org/10.1093/comjnl/7.2.149).
- 62 M. Z. Ahmad, H. Pelletier, V. Martin-Gil, *et al.*, Chemical crosslinking of 6FDA-ODA and 6FDA-ODA:DABA for improved CO<sub>2</sub>/CH<sub>4</sub> separation, *Membranes*, 2018, **8**(3), 67, DOI: [10.3390/membranes8030067](https://doi.org/10.3390/membranes8030067).
- 63 M. Zamidi Ahmad, M. Navarro, M. Lhotka, *et al.*, Enhancement of CO<sub>2</sub>/CH<sub>4</sub> separation performances of 6FDA-based co-polyimides mixed matrix membranes embedded with UiO-66 nanoparticles, *Sep. Purif. Technol.*, 2018, **192**(October 2017), 465–474, DOI: [10.1016/j.seppur.2017.10.039](https://doi.org/10.1016/j.seppur.2017.10.039).
- 64 O. G. Nik, X. Y. Chen and S. Kaliaguine, Functionalized metal organic framework-polyimide mixed matrix membranes for CO<sub>2</sub>/CH<sub>4</sub> separation, *J. Membr. Sci.*, 2012, **413**–**414**, DOI: [10.1016/j.memsci.2012.04.003](https://doi.org/10.1016/j.memsci.2012.04.003).

- 65 C. Lee, J. Seo, Y. Shul, *et al.*, Optical Properties of Polyimide Thin Films. Effect of Chemical Structure and Morphology, *Polym. J.*, 2003, **35**(7), 578–585, DOI: [10.1295/polymj.35.578](https://doi.org/10.1295/polymj.35.578).
- 66 S. J. Chen, C. Y. Li, Q. Wang, *et al.*, Reinforcing mechanism of graphene at atomic level: Friction, crack surface adhesion and 2D geometry, *Carbon*, 2017, **114**, 557–565, DOI: [10.1016/j.carbon.2016.12.034](https://doi.org/10.1016/j.carbon.2016.12.034).
- 67 Y. Liu, F. Wang, T. Tan, *et al.*, Study of the properties of molecularly imprinted polymers by computational and conformational analysis, *Anal. Chim. Acta*, 2007, **581**(1), 137–146, DOI: [10.1016/j.aca.2006.08.015](https://doi.org/10.1016/j.aca.2006.08.015).
- 68 I. Alkorta, I. Mata, E. Molins, *et al.*, Charged versus Neutral Hydrogen-Bonded Complexes: Is There a Difference in the Nature of the Hydrogen Bonds?, *Chem.–Eur. J.*, 2016, **22**(27), 9226–9234, DOI: [10.1002/chem.201600788](https://doi.org/10.1002/chem.201600788).
- 69 K. Golzar, H. Modarress and S. Amjad-Iranagh, Separation of gases by using pristine, composite and nanocomposite polymeric membranes: a molecular dynamics simulation study, *J. Membr. Sci.*, 2017, **539**, 238–256, DOI: [10.1016/j.memsci.2017.06.010](https://doi.org/10.1016/j.memsci.2017.06.010).
- 70 M. Dehghani, M. Asghari, A. F. Ismail, *et al.*, Molecular dynamics and Monte Carlo simulation of the structural properties, diffusion and adsorption of poly (amide-6-b-ethylene oxide)/Faujasite mixed matrix membranes, *J. Mol. Liq.*, 2017, **242**, 404–415, DOI: [10.1016/j.molliq.2017.07.034](https://doi.org/10.1016/j.molliq.2017.07.034).
- 71 C.-L. Lee, H. L. Chapman, M. E. Cifuentes, *et al.*, Effects of Polymer Structure on the Gas Permeability of Silicone Membranes, *J. Membr. Sci.*, 1998, **38**(1), 55–70, DOI: [10.1016/S0376-7388\(00\)83275-5](https://doi.org/10.1016/S0376-7388(00)83275-5).
- 72 Y. Yampolskii, I. Pinnau and B. D. Freeman, *Materials Science of Membranes for Gas and Vapor Separation*, 2006, pp. 437–445, DOI: [10.1002/047002903X](https://doi.org/10.1002/047002903X).
- 73 S. J. Antoniadis, C. T. Samara and D. N. Theodorou, Effect of tacticity on the molecular dynamics of polypropylene melts, *Macromolecules*, 1999, **32**(25), 8635–8644, DOI: [10.1021/ma990888f](https://doi.org/10.1021/ma990888f).
- 74 Z. Liu, Y. Liu, W. Qiu, *et al.*, Molecularly Engineered 6FDA-Based Polyimide Membranes for Sour Natural Gas Separation, *Angew. Chem., Int. Ed.*, 2020, **59**(35), 14877–14883, DOI: [10.1002/anie.202003910](https://doi.org/10.1002/anie.202003910).
- 75 M. Dehghani, M. Asghari, A. H. Mohammadi, *et al.*, Molecular simulation and Monte Carlo study of structural-transport-properties of PEBA-MFI zeolite mixed matrix membranes for CO<sub>2</sub>, CH<sub>4</sub> and N<sub>2</sub> separation, *Comput. Chem. Eng.*, 2017, **103**, 12–22, DOI: [10.1016/j.compchemeng.2017.03.002](https://doi.org/10.1016/j.compchemeng.2017.03.002).
- 76 S. Affolter, A. Ritter and M. Schmid, Interlaboratory Tests on Polymers by Differential Scanning Calorimetry (DSC): Determination of Glass Transition Temperature (T<sub>g</sub>), *Macromol. Mater. Eng.*, 2001, **286**(10), 605–610, DOI: [10.1002/1439-2054\(20011001\)286:10%3C605::AID-MAME605%3E3.0.CO;2-Y](https://doi.org/10.1002/1439-2054(20011001)286:10%3C605::AID-MAME605%3E3.0.CO;2-Y).
- 77 C. Gerstl, M. Brodeck, G. J. Schneider, *et al.*, Short and intermediate range order in poly(alkylene oxide)s. a neutron diffraction and molecular dynamics simulation study, *Macromolecules*, 2012, **45**(17), 7293–7303, DOI: [10.1021/ma301197y](https://doi.org/10.1021/ma301197y).
- 78 K. L. Tung, K. T. Lu, R. C. Ruaan, *et al.*, MD and MC simulation analyses on the effect of solvent types on accessible free volume and gas sorption in PMMA membranes, *Desalination*, 2006, **192**(1–3), 391–400, DOI: [10.1016/j.desal.2005.08.018](https://doi.org/10.1016/j.desal.2005.08.018).
- 79 K. Ghosal and B. D. Freeman, Polymers for Advanced Technologies Gas Separation Using Polymer Membranes: An Overview, *Polym. Adv. Technol.*, 1994, **5**(11), 673–697, DOI: [10.1002/pat.1994.220051102](https://doi.org/10.1002/pat.1994.220051102).
- 80 K. S. Fa and E. K. Lenzi, Power law diffusion coefficient and anomalous diffusion: Analysis of solutions and first passage time, *Phys. Rev. E: Stat. Phys., Plasmas, Fluids, Relat. Interdiscip. Top.*, 2003, **67**(6), 7, DOI: [10.1103/PhysRevE.67.061105](https://doi.org/10.1103/PhysRevE.67.061105).
- 81 V. Saenko, V. N. Kovalnogov, R. V. Fedorov, *et al.*, Numerical Method for Solving of the Anomalous Diffusion Equation Based on a Local Estimate of the Monte Carlo Method, *Mathematics*, 2022, **10**(3), 511, DOI: [10.3390/math10030511](https://doi.org/10.3390/math10030511).
- 82 J. K. Mitchell, On the Penetrativeness of Fluids, *J. Am. Chem. Soc.*, 1995, **100**(1), 11–16, DOI: [10.1016/0376-7388\(94\)00227-P](https://doi.org/10.1016/0376-7388(94)00227-P).
- 83 K. Ghosal and B. D. Freeman, Gas separation using polymer membranes: an overview, *Polym. Adv. Technol.*, 1994, **5**(11), 673–697, DOI: [10.1002/pat.1994.220051102](https://doi.org/10.1002/pat.1994.220051102).
- 84 L. Zhang, Y. Xiao, T. S. Chung, *et al.*, Mechanistic understanding of CO<sub>2</sub>-induced plasticization of a polyimide membrane: A combination of experiment and simulation study, *Polymer*, 2010, **51**(19), 4439–4447, DOI: [10.1016/j.polymer.2010.07.032](https://doi.org/10.1016/j.polymer.2010.07.032).
- 85 M. Najafi, M. Sadeghi, A. Bolverdi, *et al.*, Gas permeation properties of cellulose acetate/silica nanocomposite membrane, *Adv. Polym. Technol.*, 2018, **37**(6), 2043–2052, DOI: [10.1002/adv.21862](https://doi.org/10.1002/adv.21862).
- 86 X. R. Zhang, L. Z. Zhang and L. X. Pei, Sorption, permeation and selective transport of moisture/VOCs through a CA membrane for total heat recovery, *Int. J. Low-Carbon Technol.*, 2013, **8**(1), 64–69, DOI: [10.1093/ijlct/cts022](https://doi.org/10.1093/ijlct/cts022).
- 87 A. Hatami, I. Salahshoori, N. Rashidi, *et al.*, The effect of ZIF-90 particle in Pebax/Psf composite membrane on the transport properties of CO<sub>2</sub>, CH<sub>4</sub> and N<sub>2</sub> gases by Molecular Dynamics Simulation method, *Chin. J. Chem. Eng.*, 2020, **28**(9), 2267–2284, DOI: [10.1016/j.cjche.2019.12.011](https://doi.org/10.1016/j.cjche.2019.12.011).
- 88 Y. Zhang, Y. Wang, Y. Li, *et al.*, The mechanical properties of poly (urea-formaldehyde) incorporated with nano-SiO<sub>2</sub> by molecular dynamics simulation, *Polymers*, 2019, **11**(9), 1447, DOI: [10.3390/polym11091447](https://doi.org/10.3390/polym11091447).
- 89 C. Lee, J. Seo and Y. Shul, Optical Properties of Polyimide Thin Films. Effect of Chemical Structure and Morphology, *Polym. J.*, 2003, **35**, 578–585, DOI: [10.1295/polymj.35.578](https://doi.org/10.1295/polymj.35.578).
- 90 M. Zamidi Ahmad, M. Navarro, M. Lhotka, *et al.*, Enhancement of CO<sub>2</sub>/CH<sub>4</sub> separation performances of 6FDA-based co-polyimides mixed matrix membranes embedded with UiO-66 nanoparticles, *Sep. Purif. Technol.*, 2018, **192**, 465–474, DOI: [10.1016/j.seppur.2017.10.039](https://doi.org/10.1016/j.seppur.2017.10.039).



- 91 K. Olonisakin, M. fan, Z. Xin-Xiang, *et al.*, Key Improvements in Interfacial Adhesion and Dispersion of Fibers/Fillers in Polymer Matrix Composites; Focus on PLA Matrix Composites, *Compos. Interfaces*, 2022, **29**(10), 1071–1120, DOI: [10.1080/09276440.2021.1878441](#).
- 92 X. Qin, W. Xia, R. Sinko, *et al.*, Tuning Glass Transition in Polymer Nanocomposites with Functionalized Cellulose Nanocrystals through Nanoconfinement, *Nano Lett.*, 2015, **15**(10), 6738–6744, DOI: [10.1021/acs.nanolett.5b02588](#).
- 93 A. Y. Alentiev, G. N. Bondarenko, Y. V. Kostina, *et al.*, PIM-1/MIL-101 hybrid composite membrane material: Transport properties and free volume, *Pet. Chem.*, 2014, **54**(7), 477–481, DOI: [10.1134/S0965544114070020](#).
- 94 T. L. Chew, S. H. Ding and P. C. Oh, Functionalized KIT-6/Polysulfone Mixed Matrix, *Polymers*, 2020, **12**(10), 2312, DOI: [10.3390/polym12102312](#).
- 95 S. Mashhadikhan, A. E. Amooghin, A. Moghadassi, *et al.*, Functionalized filler/synthesized 6FDA-Durene high performance mixed matrix membrane for CO<sub>2</sub> separation, *J. Ind. Eng. Chem.*, 2021, **93**, 482–494, DOI: [10.1016/J.JIEC.2020.10.033](#).
- 96 H. Vinh-Thang and S. Kaliaguine, Predictive Models for Mixed-Matrix Membrane Performance: A Review, *Chem. Rev.*, 2013, **113**(7), 4980–5028, DOI: [10.1021/cr3003888](#).
- 97 R. Mahajan, R. Burns, M. Schaeffer, *et al.*, Challenges in forming successful mixed matrix membranes with rigid polymeric materials, *J. Appl. Polym. Sci.*, 2002, **86**(4), 881–890, DOI: [10.1002/app.10998](#).
- 98 Z. Huang, Y. Li, R. Wen, *et al.*, Enhanced gas separation properties by using nanostructured PES-zeolite 4A mixed matrix membranes, *J. Appl. Polym. Sci.*, 2006, **101**(6), 3800–3805, DOI: [10.1002/app.24041](#).
- 99 J. S. Ahn, S. H. Park, N. Y. Kwon, *et al.*, Physical properties of thermally crosslinked fluorinated polyimide and its application to a liquid crystal alignment layer, *Polymers*, 2021, **13**(22), 3903, DOI: [10.3390/polym13223903](#).
- 100 S. Xiao, R. Y. M. Huang and X. Feng, Synthetic 6FDA-ODA copolyimide membranes for gas separation and pervaporation: functional groups and separation properties, *Polymer*, 2007, **48**(18), 5355–5368, DOI: [10.1016/j.polymer.2007.07.010](#).
- 101 P. Diblíková, P. Sysel and P. Čapek, Mixed-matrix membranes based on 6FDA-ODA polyimide and silicalite-1 with homogeneous spatial distribution of particles, *Polymer*, 2019, **178**, 121576, DOI: [10.1016/j.polymer.2019.121576](#).
- 102 M. Loloï, S. Kaliaguine and D. Rodrigue, Mixed matrix membranes based on NH<sub>2</sub>-MIL-53 (Al) and 6FDA-ODA polyimide for CO<sub>2</sub> separation: Effect of the processing route on improving MOF-polymer interfacial interaction, *Sep. Purif. Technol.*, 2021, **270**, 118786, DOI: [10.1016/j.seppur.2021.118786](#).
- 103 C. Casado-Coterillo, A. Fernández-Barquín, B. Zornoza, *et al.*, Synthesis and characterisation of MOF/ionic liquid/chitosan mixed matrix membranes for CO<sub>2</sub>/N<sub>2</sub> separation, *RSC Adv.*, 2015, **5**(124), 102350–102361, DOI: [10.1039/c5ra19331a](#).
- 104 Y. Tang, S. Tang and T. Zhang, Homogeneous preparation of aerocellulose grafted acrylamide and its CO<sub>2</sub> adsorption properties, *Cellulose*, 2020, **27**(6), 3263–3275, DOI: [10.1007/s10570-020-03009-9](#).
- 105 Z. Yang, H. Peng, W. Wang, *et al.*, Imidazolium Salts as Liquid Coupling Agents for the Preparation of Polypropylene-Silica Composites, *J. Appl. Polym. Sci.*, 2010, **116**(5), 2658–2667, DOI: [10.1002/app](#).
- 106 S. N. A. Shafie, W. X. Liew, N. A. H. Md Nordin, *et al.*, CO<sub>2</sub>-philic [emim][Tf<sub>2</sub>N] modified silica in mixed matrix membrane for high performance CO<sub>2</sub>/CH<sub>4</sub> separation, *Adv. Polym. Technol.*, 2019, 2924961, DOI: [10.1155/2019/2924961](#).
- 107 J. Han, L. Bai, S. Luo, *et al.*, Ionic liquid cobalt complex as O<sub>2</sub> carrier in the PIM-1 membrane for O<sub>2</sub>/N<sub>2</sub> separation, *Sep. Purif. Technol.*, 2020, **248**, 117041, DOI: [10.1016/j.seppur.2020.117041](#).
- 108 J. G. Wijmans and R. W. Baker, The Solution-Diffusion Model: A Review, *J. Membr. Sci.*, 1995, **107**(1–2), 1–21, DOI: [10.1016/0376-7388\(95\)00102-1](#).
- 109 Z. Dai, L. Ansaloni, D. L. Gin, *et al.*, Facile fabrication of CO<sub>2</sub> separation membranes by cross-linking of poly(ethylene glycol) diglycidyl ether with a diamine and a polyamine-based ionic liquid, *J. Membr. Sci.*, 2017, **523**, 551–560, DOI: [10.1016/j.memsci.2016.10.026](#).
- 110 D.-Y. Koh and R. P. Lively, Nonporous Graphene Membranes at the limit, *Nat. Nanotechnol.*, 2015, **10**, 385–386, DOI: [10.1038/nnano.2015.77](#).
- 111 K. Asif, S. S. M. Lock, S. A. A. Taqvi, *et al.*, A molecular simulation study of silica/polysulfone mixed matrix membrane for mixed gas separation, *Polymers*, 2021, **13**(13), 2199, DOI: [10.3390/polym13132199](#).
- 112 K. Friess, P. Izák, M. Kárászová, *et al.*, A Review on Ionic Liquid Gas Separation Membranes, *Membranes*, 2021, **11**(2), 97, DOI: [10.3390/membranes11020097](#).
- 113 N. N. R. Ahmad, C. P. Leo, A. W. Mohammad, *et al.*, Recent progress in the development of ionic liquid-based mixed matrix membrane for CO<sub>2</sub> separation: a review, *Int. J. Energy Res.*, 2021, **45**(7), 9800–9830, DOI: [10.1002/er.6518](#).
- 114 X. Y. Chen and S. Kaliaguine, Mixed gas and pure gas transport properties of copolyimide membranes, *J. Appl. Polym. Sci.*, 2013, **128**(1), 380–389, DOI: [10.1002/app.37728](#).
- 115 S. E. Kentish, C. A. Scholes and G. W. Stevens, Carbon Dioxide Separation through Polymeric Membrane Systems for Flue Gas Applications, *Recent Pat. Chem. Eng.*, 2010, **1**(1), 52–66, DOI: [10.2174/1874478810801010052](#).
- 116 M. Sadeghi, M. A. Semsarzadeh and H. Moadel, Enhancement of the gas separation properties of polybenzimidazole (PBI) membrane by incorporation of silica nano particles, *J. Membr. Sci.*, 2009, **331**(1–2), 21–30, DOI: [10.1016/J.MEMSCI.2008.12.073](#).
- 117 N. Jusoh, Y. F. Yeong, K. K. Lau, *et al.*, Enhanced gas separation performance using mixed matrix membranes containing zeolite T and 6FDA-durene polyimide, *J. Membr. Sci.*, 2017, **525**, 175–186, DOI: [10.1016/j.memsci.2016.10.044](#).



- 118 M. Sadrzadeh, M. Amirilargani, K. Shahidi, *et al.*, Gas permeation through a synthesized composite PDMS/PES membrane, *J. Membr. Sci.*, 2009, **342**(1–2), 236–250, DOI: [10.1016/j.memsci.2009.06.047](https://doi.org/10.1016/j.memsci.2009.06.047).
- 119 D. F. Mohshim, H. Mukhtar, B. K. Dutta, *et al.*, Predicting CO<sub>2</sub> Permeation through an Enhanced Ionic Liquid Mixed Matrix Membrane (IL3M), *Int. J. Chem. Eng.*, 2019, **2019**, 9525783, DOI: [10.1155/2019/9525783](https://doi.org/10.1155/2019/9525783).
- 120 W. U. Mulk, S. A. Ali, S. N. Shah, *et al.*, Breaking Boundaries in CO<sub>2</sub> Capture: Ionic Liquid-Based Membrane Separation for Post-Combustion Applications, *J. CO<sub>2</sub> Util.*, 2023, **75**, 1–30, DOI: [10.1016/j.jcou.2023.102555](https://doi.org/10.1016/j.jcou.2023.102555).
- 121 T. Song, X. Zhang, Y. Li, *et al.*, Separation Efficiency of CO<sub>2</sub> in Ionic Liquids/Poly(vinylidene fluoride) Composite Membrane: A Molecular Dynamics Study, *Ind. Eng. Chem. Res.*, 2019, **58**(16), 6887–6898, DOI: [10.1021/acs.iecr.8b06100](https://doi.org/10.1021/acs.iecr.8b06100).
- 122 P. S. Goh, A. F. Ismail, S. M. Sanip, *et al.*, Recent advances of inorganic fillers in mixed matrix membrane for gas separation, *Sep. Purif. Technol.*, 2011, **81**(3), 243–264, DOI: [10.1016/j.seppur.2011.07.042](https://doi.org/10.1016/j.seppur.2011.07.042).
- 123 X. Zhang, T. Zhang, Y. Wang, *et al.*, Mixed-matrix membranes based on Zn/Ni-ZIF-8-PEBA for high performance CO<sub>2</sub> separation, *J. Membr. Sci.*, 2018, **560**(April), 38–46, DOI: [10.1016/j.memsci.2018.05.004](https://doi.org/10.1016/j.memsci.2018.05.004).
- 124 Y. Shen, H. Wang, X. Zhang, *et al.*, MoS<sub>2</sub> nanosheets functionalized composite mixed matrix membrane for enhanced CO<sub>2</sub> capture via surface drop-coating method, *ACS Appl. Mater. Interfaces*, 2016, **8**(35), 23371–23378, DOI: [10.1021/acsami.6b07153](https://doi.org/10.1021/acsami.6b07153).
- 125 H. Lin and B. D. Freeman, Gas solubility, diffusivity and permeability in poly(ethylene oxide), *J. Membr. Sci.*, 2004, **239**(1), 105–117, DOI: [10.1016/j.memsci.2003.08.031](https://doi.org/10.1016/j.memsci.2003.08.031).
- 126 C. Casado-Coterillo, A. Fernández-Barquín and A. Irabien, Effect of humidity on CO<sub>2</sub>/N<sub>2</sub> and CO<sub>2</sub>/CH<sub>4</sub> separation using novel robust mixed matrix composite hollow fiber membranes: Experimental and model evaluation, *Membranes*, 2020, **10**(1), 6, DOI: [10.3390/membranes10010006](https://doi.org/10.3390/membranes10010006).
- 127 M. Sadeghi, M. A. Semsarzadeh and H. Moadel, Enhancement of the gas separation properties of polybenzimidazole (PBI) membrane by incorporation of silica nano particles, *J. Membr. Sci.*, 2009, **331**(1–2), 21–30, DOI: [10.1016/j.memsci.2008.12.073](https://doi.org/10.1016/j.memsci.2008.12.073).
- 128 T. S. Chung, L. Y. Jiang, Y. Li, *et al.*, Mixed Matrix Membranes (MMMs) Comprising Organic Polymers with Dispersed Inorganic Fillers for Gas Separation, *Prog. Polym. Sci.*, 2007, **32**(4), 483–507, DOI: [10.1016/j.progpolymsci.2007.01.008](https://doi.org/10.1016/j.progpolymsci.2007.01.008).
- 129 M. Safak Boroglu and A. B. Yumru, Gas separation performance of 6FDA-DAM-ZIF-11 mixed-matrix membranes for H<sub>2</sub>/CH<sub>4</sub> and CO<sub>2</sub>/CH<sub>4</sub> separation, *Sep. Purif. Technol.*, 2017, **173**, 269–279, DOI: [10.1016/j.seppur.2016.09.037](https://doi.org/10.1016/j.seppur.2016.09.037).
- 130 T. T. Moore and W. J. Koros, Non-ideal effects in organic-inorganic materials for gas separation membranes, *J. Mol. Struct.*, 2005, **739**(1–3), 87–98, DOI: [10.1016/j.molstruc.2004.05.043](https://doi.org/10.1016/j.molstruc.2004.05.043).
- 131 S. H. Han, H. J. Kwon, K. Y. Kim, *et al.*, Tuning microcavities in thermally rearranged polymer membranes for CO<sub>2</sub> capture, *Phys. Chem. Chem. Phys.*, 2012, **14**(13), 4365–4373, DOI: [10.1039/c2cp23729f](https://doi.org/10.1039/c2cp23729f).
- 132 M. I. F. Zainuddin and A. L. Ahmad, Mixed Matrix Membrane Development Progress and Prospect of Using 2D Nanosheet Filler for CO<sub>2</sub> separation and Capture, *J. CO<sub>2</sub> Util.*, 2022, **62**, 102094, DOI: [10.1016/j.jcou.2022.102094](https://doi.org/10.1016/j.jcou.2022.102094).
- 133 T. Corrado and R. Guo, Macromolecular Design Strategies toward Tailoring Free Volume in Glassy Polymers for High Performance Gas Separation Membranes, *Mol. Syst. Des. Eng.*, 2020, **5**(1), 22–48, DOI: [10.1039/c9me00099b](https://doi.org/10.1039/c9me00099b).
- 134 R. Nasir, N. N. R. Ahmad, H. Mukhtar, *et al.*, Effect of ionic liquid inclusion and amino-functionalized SAPO-34 on the performance of mixed matrix membranes for CO<sub>2</sub>/CH<sub>4</sub> separation, *J. Environ. Chem. Eng.*, 2018, **6**(2), 2363–2368, DOI: [10.1016/j.jece.2018.03.032](https://doi.org/10.1016/j.jece.2018.03.032).
- 135 N. N. R. Ahmad, C. P. Leo and A. L. Ahmad, Effects of solvent and ionic liquid properties on ionic liquid enhanced polysulfone/SAPO-34 mixed matrix membrane for CO<sub>2</sub> removal, *Microporous Mesoporous Mater.*, 2019, **283**, 64–72, DOI: [10.1016/j.micromeso.2019.04.001](https://doi.org/10.1016/j.micromeso.2019.04.001).
- 136 D. D. Iarikov, P. Hacırlıoğlu and S. T. Oyama, Supported room temperature ionic liquid membranes for CO<sub>2</sub>/CH<sub>4</sub> separation, *Chem. Eng. J.*, 2011, **166**(1), 401–406, DOI: [10.1016/j.cej.2010.10.060](https://doi.org/10.1016/j.cej.2010.10.060).
- 137 K. Kumar and A. Kumar, Enhanced CO<sub>2</sub> Adsorption and Separation in Ionic-Liquid-Impregnated Mesoporous Silica MCM-41: A Molecular Simulation Study, *J. Phys. Chem. C*, 2018, **122**(15), 8216–8227, DOI: [10.1021/acs.jpcc.7b11529](https://doi.org/10.1021/acs.jpcc.7b11529).
- 138 K. Kumar and A. Kumar, Enhanced CO<sub>2</sub> Adsorption and Separation in Ionic-Liquid-Impregnated Mesoporous Silica MCM-41: A Molecular Simulation Study, *J. Phys. Chem. C*, 2018, **122**(15), 8216–8227, DOI: [10.1021/acs.jpcc.7b11529](https://doi.org/10.1021/acs.jpcc.7b11529).
- 139 K. Donato, L. Matějka, R. Mauler, *et al.*, Recent Applications of Ionic Liquids in the Sol-Gel Process for Polymer–Silica Nanocomposites with Ionic Interfaces, *Colloids Interfaces*, 2017, **1**(1), 5, DOI: [10.3390/colloids1010005](https://doi.org/10.3390/colloids1010005).
- 140 S. Ding, X. Li, S. Ding, *et al.*, Ionic liquid-decorated nanocages for cooperative CO<sub>2</sub> transport in mixed matrix membranes, *Sep. Purif. Technol.*, 2020, **239**, 116539, DOI: [10.1016/j.seppur.2020.116539](https://doi.org/10.1016/j.seppur.2020.116539).
- 141 B. Liu, D. Li, J. Yao, *et al.*, Improved CO<sub>2</sub> separation performance and interfacial affinity of mixed matrix membrane by incorporating UiO-66-PEI@[bmim][Tf<sub>2</sub>N] particles, *Sep. Purif. Technol.*, 2020, **239**, 116519, DOI: [10.1016/j.seppur.2020.116519](https://doi.org/10.1016/j.seppur.2020.116519).
- 142 K. R. Raj and A. R. Sunarti, Preliminary Fractional Factorial Design (FFD) Study Using Incorporation of Graphene Oxide in PVC in Mixed Matrix Membrane to Enhance CO<sub>2</sub>/CH<sub>4</sub> Separation, *IOP Conf. Ser.: Mater. Sci. Eng.*, 2019, **702**, 012041, DOI: [10.1088/1757-899X/702/1/012041](https://doi.org/10.1088/1757-899X/702/1/012041).

- 143 K. M. Gupta, Y. Chen, Z. Hu, *et al.*, Metal-organic framework supported ionic liquid membranes for CO<sub>2</sub> capture: anion effects, *Phys. Chem. Chem. Phys.*, 2012, **14**(16), 5785–5794, DOI: [10.1039/c2cp23972h](https://doi.org/10.1039/c2cp23972h).
- 144 J. L. Anthony, J. L. Anderson, E. J. Maginn, *et al.*, Anion Effects on Gas Solubility in Ionic Liquids, *J. Phys. Chem. B*, 2005, **109**(13), 6366–6374, DOI: [10.1021/jp046404l](https://doi.org/10.1021/jp046404l).
- 145 I. Yasmeeen, A. Ilyas, Z. Shamair, *et al.*, Synergistic effects of highly selective ionic liquid confined in nanocages: exploiting the three component mixed matrix membranes for CO<sub>2</sub> capture, *Chem. Eng. Res. Des.*, 2020, **155**, 123–132, DOI: [10.1016/j.cherd.2020.01.006](https://doi.org/10.1016/j.cherd.2020.01.006).
- 146 S. Duan, T. Kouketsu, S. Kazama, *et al.*, Development of PAMAM dendrimer composite membranes for CO<sub>2</sub> separation, *J. Membr. Sci.*, 2006, **283**(1–2), 2–6, DOI: [10.1016/j.memsci.2006.06.026](https://doi.org/10.1016/j.memsci.2006.06.026).
- 147 C. Wang and R. Patel, Recent Advances on Ionic Liquid based Mixed Matrix Membrane for CO<sub>2</sub> Separation, *Membr. J.*, 2021, **31**(1), 1–15, DOI: [10.14579/MEMBRANE\\_JOURNAL.2021.31.1.1](https://doi.org/10.14579/MEMBRANE_JOURNAL.2021.31.1.1).